

PACS photometer point spread function

Dieter Lutz

Contents

1	Summary	2
2	Data reference sheet	3
3	Description of observations	3
4	Analysis methods and dp scripts used	4
5	Results	6
5.1	PSF morphology	6
5.2	PSF morphology at faint levels	10
5.3	Comparison to modelled PSFs	13
6	Impact of saturation, crosstalk, ghosts and straylight on observed PSF	19
6.1	Saturation aftereffects	19
6.2	Detector crosstalk	19
6.3	Ghosts in blue array	20
6.4	Blue streaks, other reflections and straylight effects	21
6.5	Implications of peculiar effects	26
7	Effects of data reduction methods and of source SED	27
7.1	Effects of highpass filtering	27
7.2	Standard data reduction vs. recentering	27
7.3	Effects of source SED	27
7.4	Effects of drizzling	29
8	Encircled energy diagrams	32
8.1	Ancillary information	33
8.2	Derivation of EEf curves	34
9	Data products accompanying this note	40
10	Related documents	41
11	Document change record	42

1 Summary

The PACS Performance Verification (PV) and routine calibration plan includes a broad range of observations aiming to characterise the PSF for a wide range of observing modes and source SEDs. The SED distinction is made because of the expected dependence of PSF width on SED slope, which is due the wide filter bandpasses.

Version 1.0 of this note presents results derived from scanmap observations during various PV and routine phase calibrations using the star α Tau and the asteroid Vesta. Both are ‘hot’ sources for PACS, with different flux levels but within the linear and unsaturated flux range. Mars, Neptune, IK Tau and the Red Rectangle are used as extremely bright targets for characterizing PSF wings and to probe for ghosts and straylight. This is done realizing they are not point sources and may be nonlinear or saturated in parts of the PSF cores.

A final PSF characterisation will use a yet wider set of observations and make use of calibrations and reduction steps that are currently not yet available. PSF images for Vesta are released along with this note. *We emphasize that the true PSF of a given science observation may differ in detail from what is presented here.* Such variations may occur for the PSF core due to pointing jitter during the scans and *in particular due to specific data reduction steps taken.* Variations from observation to observation are also possible for the faintest PSF wings since some of the crosstalk/straylight/ghost effects discussed below vary with the exact path the source has taken across the PACS arrays.

The photometer PSF is characterised by

- A narrow core which is round in the blue and green bands but slightly elongated in spacecraft Z direction¹ in red.
- A tri-lobe pattern seen at the several % level in all bands, most clearly in the blue with its strongest signal. It is ascribed to imperfect shape of the Herschel primary mirror.
- Knotty structure at sub-percent level, clearly seen in blue and green.

For fast scans in normal and parallel mode, this PSF structure is smeared in scan direction by detector time constants and on-board data averaging.

The most prominent unusual effects are: (1) A narrow and faint spike, extending in z direction. This spike is seen in blue and green and also indicated in red. (2) A negative PSF feature in the scan direction of blue/green fast scans which is indicative of an undershooting of the signal after source passage. (3) Negative ghost images due to detector crosstalk. (4) Several types of weak ghost reflections occurring, for example, when the source is just off the array corners.

At the faint levels of the PSF the six-spoke diffraction pattern is seen, that is caused by the secondary mirror support.

A set of PACS modelled PSFs is independently presented in document PICC-ME-TN-029, in its version 2.0 including an ‘as built’ telescope model that is implementing pre-launch knowledge on the telescope wavefront

¹For the orientation of the spacecraft Y,Z directions on sky with respect to the PACS arrays see, e.g., Fig. 11 or document PICC-ME-TN-027

errors. While these modelled PSFs reproduce many salient features of the observed PSF, they may not be realistic enough for use in tasks that require accurate PSFs, like PSF fitting and deconvolution. By definition they refer to the Herschel telescope only and will not include ghosts etc. that are arising in PACS.

2 Data reference sheet

OD	OBSID	Source	HSPOT name	sec
118	1342183538	α Tau	Calibration_PVPhotSpatial_1-PVPhotSpatial_314D_StdScan_blumed_AlfTau_0001	853
118	1342183539	α Tau	Calibration_PVPhotSpatial_1-PVPhotSpatial_314D_StdScan_bluhigh_AlfTau_0001	819
118	1342183540	α Tau	Calibration_PVPhotSpatial_1-PVPhotSpatial_314D_StdScan_blulow_AlfTau_0001	1215
118	1342183541	α Tau	Calibration_PVPhotSpatial_1-PVPhotSpatial_314D_StdScan_grnmed_AlfTau_0001	853
118	1342183542	α Tau	Calibration_PVPhotSpatial_1-PVPhotSpatial_314D_StdScan_grnhigh_AlfTau_0001	819
118	1342183543	α Tau	Calibration_PVPhotSpatial_1-PVPhotSpatial_314D_StdScan_grnlow_AlfTau_0001	1215
119	1342183556	Red Rect	Calibration_PVPhotSpatial_1-PVPhotSpatial_315B_StdScan_blu_RedRect_0001	13245
119	1342183559	IK Tau	Calibration_PVPhotSpatial_1-PVPhotSpatial_316A_StdScan_blu_IKTau_0001	6481
124	1342183880	3C345	Calibration_PVPhotSpatial_1-PVPhotSpatial_314D_StdScan_bluhigh_3C345_0001	819
124	1342183881	3C345	Calibration_PVPhotSpatial_1-PVPhotSpatial_314D_StdScan_blumed_3C345_0001	853
124	1342183882	3C345	Calibration_PVPhotSpatial_1-PVPhotSpatial_314D_StdScan_blulow_3C345_0001	1215
124	1342183883	3C345	Calibration_PVPhotSpatial_1-PVPhotSpatial_314D_StdScan_grnlow_3C345_0001	1215
124	1342183884	3C345	Calibration_PVPhotSpatial_1-PVPhotSpatial_314D_StdScan_grnmed_3C345_0001	853
124	1342183885	3C345	Calibration_PVPhotSpatial_1-PVPhotSpatial_314D_StdScan_grnhigh_3C345_0001	819
137	1342184486	Mars	Calibration_PVParStray_1-PVParStray_316A_TFOV_blu2dx2d_centre_Mars_OD137	11044
137	1342184487	Mars	Calibration_PVParStray_1-PVParStray_316A_TFOV_blu2x2d_centre_Mars_off1_OD137	11044
137	1342184488	Mars	Calibration_PVParStray_1-PVParStray_316A_TFOV_blu2x2d_centre_Mars_off2_OD137	11044
160	1342186132	Vesta	Calibration_PVPhotSpatial_1-PVPhotSpatial_314D_StdScan_grnlow_Vesta_0001	1407
160	1342186133	Vesta	Calibration_PVPhotSpatial_1-PVPhotSpatial_314D_StdScan_grnmed_Vesta_0001	1045
160	1342186134	Vesta	Calibration_PVPhotSpatial_1-PVPhotSpatial_314D_StdScan_grnhigh_Vesta_0001	1011
160	1342186135	Vesta	Calibration_PVPhotSpatial_1-PVPhotSpatial_314D_StdScan_blulow_Vesta_0001	1407
160	1342186136	Vesta	Calibration_PVPhotSpatial_1-PVPhotSpatial_314D_StdScan_blumed_Vesta_0001	1045
160	1342186137	Vesta	Calibration_PVPhotSpatial_1-PVPhotSpatial_314D_StdScan_bluhigh_Vesta_0001	1011
173	1342186639	Neptune	Calibration_PVPhotFlux_1-PVPhotFlux_321D_StdScan_045_pcal_blu_Neptune_0001	179
173	1342186640	Neptune	Calibration_PVPhotFlux_1-PVPhotFlux_321D_StdScan_135_pcal_blu_Neptune_0001	179
173	1342186641	Neptune	Calibration_PVPhotFlux_1-PVPhotFlux_321D_StdScan_045_pcal_grn_Neptune_0001	179
173	1342186642	Neptune	Calibration_PVPhotFlux_1-PVPhotFlux_321D_StdScan_135_pcal_grn_Neptune_0001	179
345	1342195470	Vesta	Calibration_RPPhotSpatial_1-RPPhotSpatial_314A_StdScan+42_hi_blu_Vesta_0001	703
345	1342195471	Vesta	Calibration_RPPhotSpatial_1-RPPhotSpatial_314A_StdScan-42_hi_blu_Vesta_0001	703
345	1342195472	Vesta	Calibration_RPPhotSpatial_1-RPPhotSpatial_314A_StdScan+42_med_blu_Vesta_0001	741
345	1342195473	Vesta	Calibration_RPPhotSpatial_1-RPPhotSpatial_314A_StdScan-42_med_blu_Vesta_0001	741
345	1342195474	Vesta	Calibration_RPPhotSpatial_1-RPPhotSpatial_314A_StdScan+42_hi_grn_Vesta_0001	703
345	1342195475	Vesta	Calibration_RPPhotSpatial_1-RPPhotSpatial_314A_StdScan-42_hi_grn_Vesta_0001	703
345	1342195476	Vesta	Calibration_RPPhotSpatial_1-RPPhotSpatial_314A_StdScan+42_med_grn_Vesta_0001	741
345	1342195477	Vesta	Calibration_RPPhotSpatial_1-RPPhotSpatial_314A_StdScan-42_med_grn_Vesta_0001	741
348	1342195622	Vesta	Calibration_RPPhotSpatial_1-RPPhotSpatial_314B_StdScan+20_med_grn_Vesta_0001	3926

3 Description of observations

The dedicated PSF observations are scanmaps centered on the star α Tau (OD118), the asteroid Vesta (OD160), and the blazar 3C345 (OD124), using 15 scanlegs with 3 arcsec cross-scan separation. The scan orientation angle is 63 degree in the array frame, along the array diagonal. This pattern is overall providing source passages over many regions of the array and with good sub-pixel sampling. For Vesta, additional observations were taken in fast scan and at the Spire/Pacs parallel mode ‘magic’ scan orientation angles ± 42 degrees (OD345).

The fluxes of α Tau are about 14.0–6.9–2.7Jy at 70–100–160 μ m according to the PV plan PICC-MA-PL-001. The flux of Vesta during the OD160 observations was about 93–49–20Jy (T. Müller 26.10.2009). 3C345 was

measured at about 0.27–0.40–0.69 Jy.

Scanmaps of Mars (OD137, 61900–34300–15500 Jy) and Neptune (OD173, 353–357–260Jy, T. Müller, 13.8.2010) are used to investigate fainter PSF structures.

4 Analysis methods and dp scripts used

For the best fidelity PSF results we obtain ‘recentered’ PSFs by a posteriori correcting for pointing variations. Here we use two main reduction steps (1) determination of pointing corrections and (2) mapping. In other cases we use a normal processing, skipping step (1).

Pointing corrections are determined in the first pass by comparing frame per frame the expected location of the source on the array (computed from pointing product information and PACS spatial calibration) with the measured position from a 2-d gaussian fit. Only frames for which the source was centered at least 1.5 pixels inside a matrix were kept. The corrections derived were then used in the second pass processing to adjust the input RA, DEC coordinates of each frame to achieve consistency between expected and actual centroid on the frame. Given instantaneous S/N in the respective filters, corrections were derived from the blue/green data and applied also to the red data, considering the time shift of the frame indices in each camera. This procedure was applied only to the α Tau and Vesta data. By definition, it produces small PSF images reaching away from the source by at most an array size, since the source has to be on the array for derivation of the recentering correction. By definition, it will also suppress those ghosts which are occurring while the source is off the array.

The second pass is a highpass-filtered scanmap production, making use of the corrected pointing (if recentering) or the nominal Herschel pointing otherwise:

- Calblock related steps and drift correction were bypassed. This is now also the pipeline default.
- We used 2nd-level deglitching in the timeordered mode. For Mars with its straylight and saturation effects we relaxed the detection threshold within 5arcmin and completely suppressed deglitching within 2 arcmin. Still, there are for Mars some remaining effects of deglitching e.g. in regions crossed by a detector that was previously saturated while crossing the planet, and now showing aftereffects of the saturation.
- Coverage maps were checked and had no dips at the source position any more, except for saturated sources. Coverage dips are often present in the region separated by one matrix size from the source which is affected by crosstalk. Since this crosstalk is seen in only part of the pixels that crossed a given spot on sky, it is identified by the 2nd level deglitching if the source is bright.
- A region centered on the source with 60 arcsec radius (α Tau, most Vesta observations) or larger (for brighter sources and larger maps) was masked in the highpass filtering to suppress the familiar filtering residues on both sides of the bright source. A highpass filter radius of 100 arcsec on sky (for 60arcsec masking radius, larger otherwise) was used.
- All maps were projected on a 1 arcsec pixel grid with a map position angle based on the spacecraft position angle at the time of the observation. As a consequence, the PSF image axes align with the spacecraft y,z directions as if the spacecraft position angle would have been 0. When we refer to ‘position angles’ of structures below these are ‘east of north’ (ccw) relative to the spacecraft z axis which is pointing upwards in the PSF images, rather than relative to the actual north direction of the particular observation. The sources are centered on a single pixel at the map center. We have enforced this pixel centering despite

Source	OD	dRA/dt deg/h	dDEC/dt deg/h
Mars	137	0.025299	-0.002823
Vesta	160	0.014853	-0.003412
Neptune	173	-0.000036	-0.000015
Vesta	345	0.004937	-0.003147
Vesta	348	0.005746	-0.003431

Table 1: Proper motions adopted for the SSO observations used in this note (based on input provided by T. Müller)

satellite pointing offsets, with the consequence that the RA, DEC of the source nominally read off the map may disagree with the literature.

- To ensure a clearly defined zero point in flux, all PSFs were explicitly corrected to “Daophot”-background 0 in an annular aperture of width 10 arcsec just outside the masking radius used. Note this has implications for the encircled energy fraction discussion below.

All the data (except Mars, which was observed in parallel mode) were taken in standard PACS prime scan mode but we partly simulate the blue/green PSF for parallel mode at 60arcsec/sec and 20arcsec/sec. Parallel mode blue/green is on-board averaging 8 rather than 4 40Hz samples. We simulate this in reduction from standard scans by averaging the fluxes and coordinates of 2 consecutive frames of our data, which were already on-board averaged for 4 samples at 40Hz.

The data for Vesta, a solar system object moving at 53arcsec/h at the time of the OD160 observations, as well as all other SSOs, were made amenable to the same processing by applying a suitable linear correction to the nominal coordinates as a function of time (Table 1).

Our reduction procedure has a number of implications on the derived PSF that are worth mentioning:

- PSFs measured in standard scanmap reductions will typically have a wider core than the recentered ones, due to pointing jitter, possibly imperfect PACS spatial calibration, and potential small synchronisation issues between data and pointing. All of these are tackled ad hoc by the recentering. The last two factors may be reduced in the future with improving calibration while the first will always remain for faint source data to some level. See section 7.2 for a quantitative example. For some of the main Vesta cases we provide both recentered PSFs, which typically will need observation-specific convolution for application to real data, and PSFs as obtained from normal processing for our particular observation.
- These PSFs represent the convolution of the telescope PSF with the PACS pixel size - PRFs in Spitzer speak. The map pixel is small in comparison to the physical PACS pixel for our adopted parameters.
- Because of redundancy introduced by the scanning, results should be more robust to current incomplete knowledge of reduction steps like flatfield, dubious pixels, crosstalk etc. than chopped/nodded observations. Nevertheless they will be subject to update in case improved flatfields or crosstalk correction methods become available.
- For fast scan and parallel mode, there could be subtle but basic differences between the PSFs derived here from several back and forth scans and using recentering, to the PSF from single pass unidirectional scans as can occur in sparsely sampled maps, because of the effects of detector time response. Section 7.2 suggests these differences are minor.

- By definition of the recentering step, the recentered PSFs will not include ghost related features arising while the source was off the array (e.g., a possible effect of the ‘blue streaks’ seen for sources just outside the array corner in FM-ILT). See also the discussion of the Mars observations below.

All PSFs presented here are based on the highpass filter / photproject reduction scheme. Cross scans for reduction with ‘madmap’ like inversion algorithms are available for a subset (OD173 Neptune, OD345 Vesta) but have not been used in this way, given the current presence of e.g. artefacts near bright sources in madmap reductions.

5 Results

Figures 1 to 3 show the resulting recentered Vesta PSF images at different linear stretches -0.05–1, -0.005–0.1 and -0.0005–0.01 times the PSF peak. α Tau results are consistent but of lower S/N. The linear noise structures in scan direction are a consequence of the fairly large width highpass filter that was used. It should be noted that at the given noise level, background sources start to be detected and are in fact seen outside the image panels shown. While formal proof that any faint feature seen is not due to a background object or real structure near α Tau or Vesta will need confirmation on several independent sources, we proceed here with the assumption that structures above the noise are PSF features. The good agreement between the two datasets from different targets supports this.

Table 2 summarizes results from fitting a 2-dimensional gaussian to the full PSF including wings. While such gaussian fits may not be an optimal representation of the PSF they allow for quick comparison with mapping results from other observations. The PSF width in blue for slow scan is similar to first results that were seen in single frame staring data, giving confidence that the recentering/mapping procedure recovers the actual PACS PSF. The agreement between the widths measured from the Vesta and α Tau datasets is very good.

5.1 PSF morphology

In all three bands the PSF core is surrounded by a tri-lobe pattern at the level of up to 10% (in blue) of the PSF peak. The optical modelling by N. Geis presented in PICC-ME-TN-029 Issue 2.0 reproduces this with the wavefront errors of the Herschel main mirror. The wavefront errors are reflecting, among other factors, the 120 degree symmetry of the secondary mirror suspensions. In all three bands, the top-right of the three lobes is observed weakest, qualitatively reproduced by the models.

The next fainter level of PSF structures is again not a clear diffraction ring but a knotty pattern at the % level and below. It is clearly seen in blue and well confirmed in the 10 vs. 20 arcsec/sec data. A similar pattern is seen in green but with less detail at current S/N.

The blue data show a weak spike in roughly vertical (spacecraft z) direction, perhaps similar to a spike seen in ILT data (FM report figure 1.124). The spike is clearly confirmed in green and perhaps also in red. Roughly 70arcsec towards the -z direction, a bright spot is superposed on this spike, clearly seen in blue and weakly in green (outside the range in Figs 1 to 3). Deeper Vesta and Neptune observations (see below) confirm the bright spot. Results discussed in section 6.3 show it is induced in PACS rather than the telescope and likely an optical

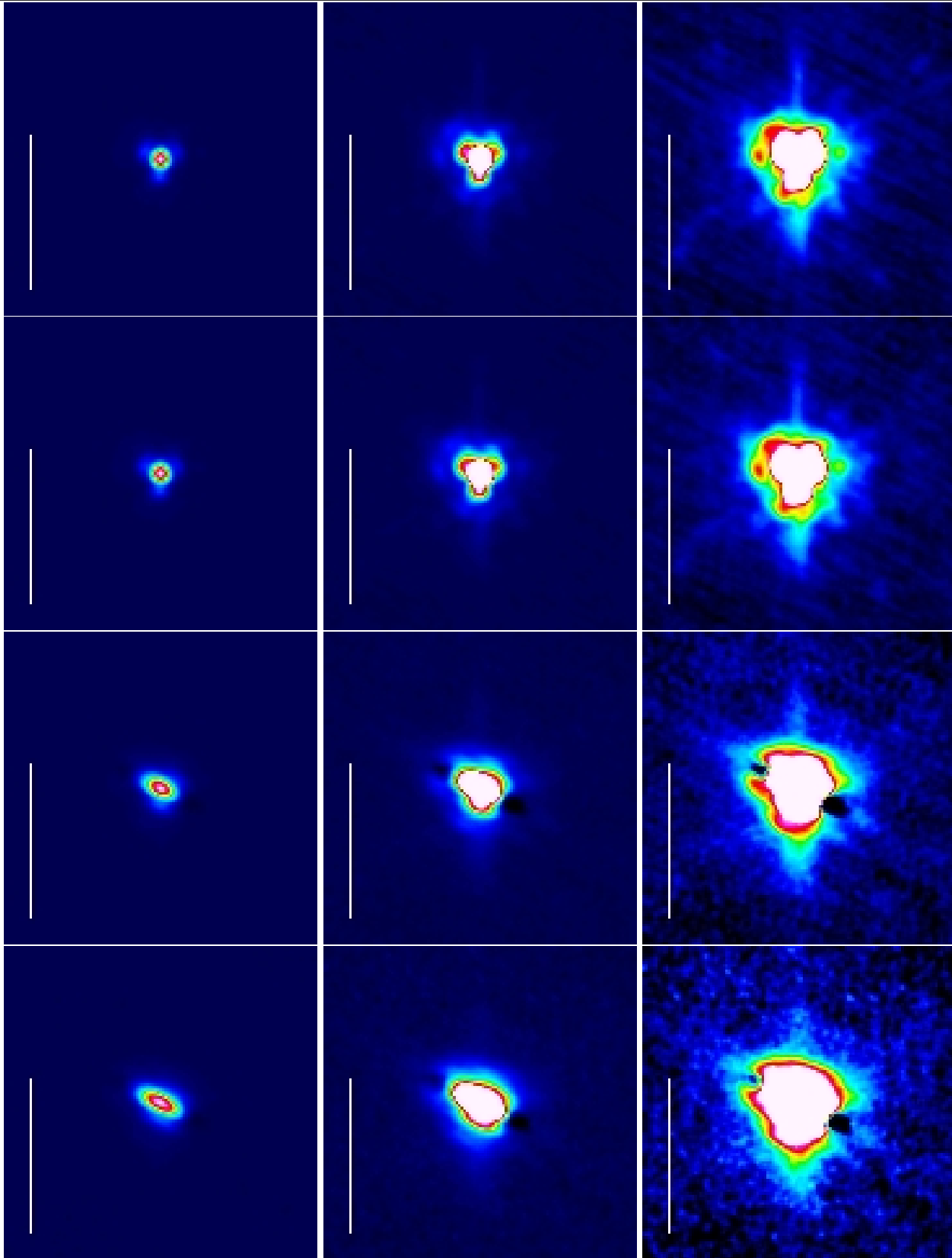


Figure 1: Blue PSF from recentered OD160 Vesta data, from left to right linearly scaled to peak, 10%, and 1% of peak. From top to bottom scanspeed 10, 20, 60 arcsec/sec and (simulated) parallel mode at 60 arcsec/sec. Spacecraft Z is on top as if PA=0. Scan orientation angle is 63deg in array coordinates. The scale bar indicates 60arcsec.

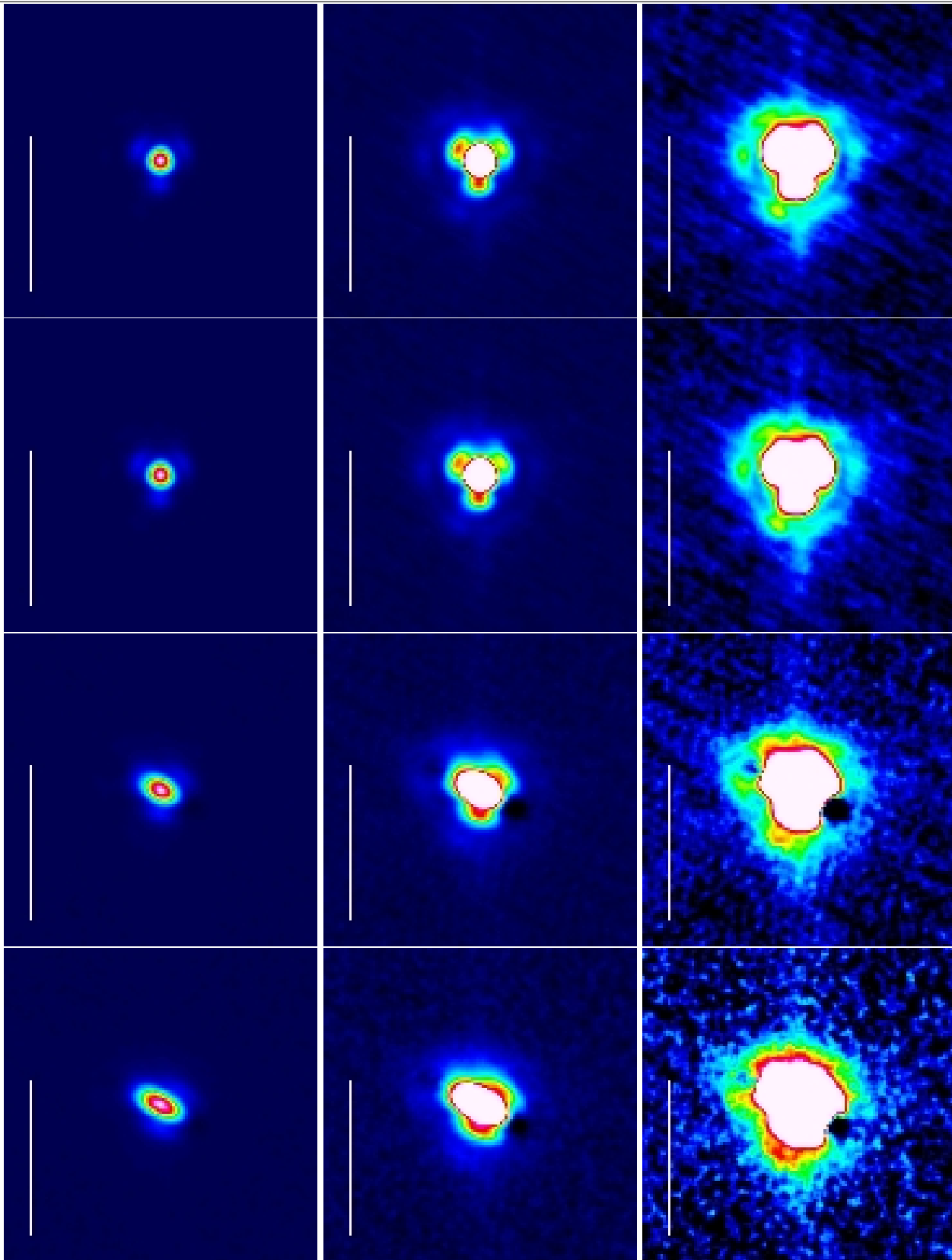


Figure 2: Green PSF from recentered OD160 Vesta data, from left to right linearly scaled to peak, 10%, and 1% of peak. From top to bottom scanspeed 10, 20, 60 arcsec/sec and (simulated) parallel mode at 60 arcsec/sec. The scale bar indicates 60arcsec.

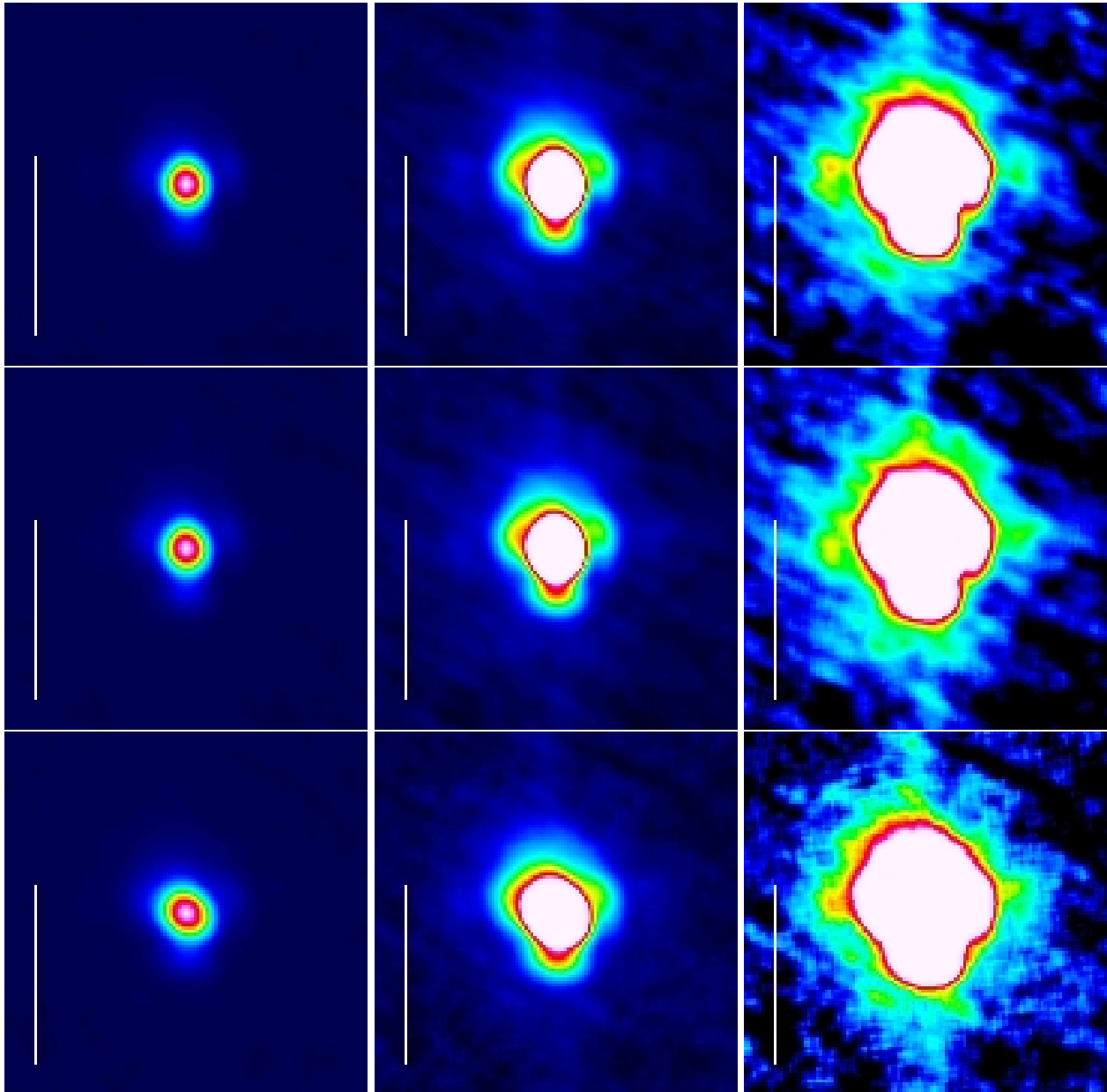


Figure 3: Red PSF from recentered OD160 Vesta data, from left to right linearly scaled to peak, 10%, and 1% of peak. From top to bottom scanspeed 10, 20, 60 arcsec/sec. For red the parallel mode sampling is identical to prime mode. The scale bar indicates 60arcsec.

ghost. The deeper observations also confirm the vertical linear feature, relative to the PSF peak it is strongest and most extended in red. In blue/green it seems shorter and asymmetric, stronger towards the +z direction (upwards).

The fast scan blue and green PSFs show a region in scan direction from the PSF peak where the flux is undershooting to below zero, to a level of about -1% of the peak. Its origin is not understood, and undershooting of the signal after a short exposure to a bright signal would be needed to create it. It is unclear to which extent this effect is (non)linear. A test reduction using a huge highpass filter width and avoiding deglitching reproduced the effect. The undershoot can already be seen in individual timelines, again demonstrating it is not a processing artefact.

At slow scan speed, the PSF fits are roughly round for blue and green but vertically elongated in the red. This elongation is seen in the PSF core and not just an effect of wings or lobes. A slight elongation in same direction was seen in ILT but cannot be compared quantitatively given the properties of the ILT setup plus its use of somewhat extended holes for the artificial source.

Comparing results for the slow scan speeds 10 and 20 arcsec/sec, the PSFs are very similar at both speeds in all bands. Fast scan and in particular blue/green parallel mode with 8-sample averaging show significant elongation in scan direction, as expected. The detailed PSF pattern for fast scan will depend on the relative orientation of scan direction and the tri-lobe pattern, the PSFs shown here can give only examples for the given scan direction relative to the array. Given the SPIRE-driven preference for the ‘magic’ scan orientation angles +42 and -42deg (array coordinates) in parallel mode, dedicated observations were obtained in OD345 at these scan orientation angles. Table 3 gives width results for these scan orientation angles. Figure 4 shows examples.

Band	Speed arcsec/sec	FWHM		PA deg	FWHM		PA deg
		Vesta OD160	arcsec		α Tau OD118	arcsec	
Blue	10	5.25×5.61			5.20×5.56		
Blue	20	5.46×5.77			5.40×5.70		
Blue	60	5.73×9.11		61.7	5.70×8.92		61.6
Blue	20/para	5.57×6.33		52.9			
Blue	60/para	5.82×12.09		62.6			
Green	10	6.53×6.78			6.52×6.76		
Green	20	6.66×6.89			6.63×6.83		
Green	60	6.83×9.82		61.7	6.84×9.66		61.8
Green	20/para	6.73×7.29		52.6			
Green	60/para	6.94×12.65		62.5			
Red	10	10.38×11.95		6.3	10.41×11.98		8.1
Red	20	10.53×12.06		9.3	10.58×12.06		9.4
Red	60	11.38×13.34		41.5	11.35×13.30		40.8

Table 2: Results of fitting 2-dimensional gaussians to the recentered PSF for Vesta and α Tau. Note these are fits to the full PSF including the lobes/wings. Position angles (east of the spacecraft z direction) are listed only for beams with clearly elongated core. *Scan orientation angle is 63deg in array coordinates for these observations.*

5.2 PSF morphology at faint levels

α Tau and Vesta are selected to be bona fide PSF sources: Effectively pointlike at PACS resolution, and having no surrounding far-infrared structure. They are still faint enough to not induce significant nonlinearities or saturation in the bolometer response. Conversely, they are not bright enough to reveal the faintest PSF levels,

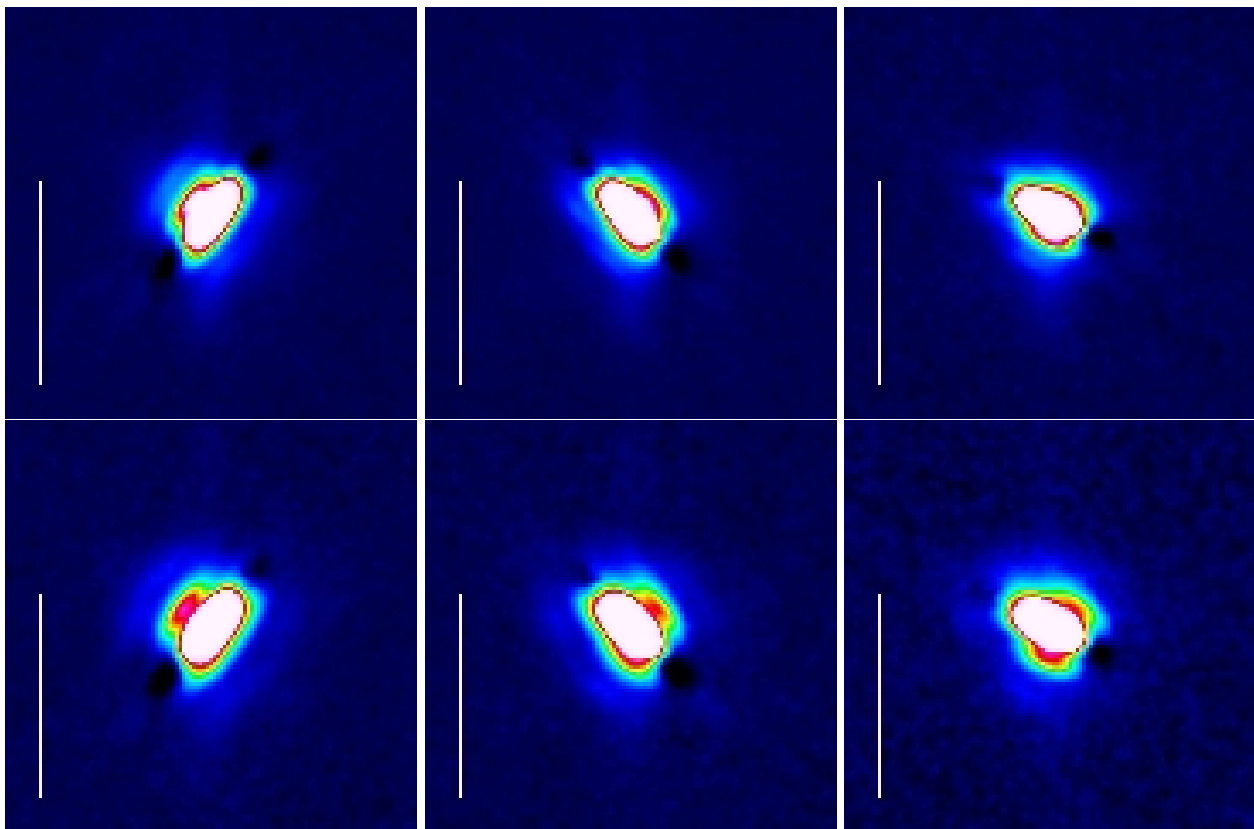


Figure 4: Example of the effect of scan PA on the PSF, shown here for fast parallel mode blue (top) and green and the three scan orientation angles -42, +42, +63degree. The alignment of true PSF features and scan smearing changes.

Band	Speed arcsec/sec	FWHM arcsec	PA deg	Scan OA	OD
Blue	20/para	5.54×6.61	30.5	+42	345
Blue	60/para	5.94×12.63	43.6	+42	345
Green	20/para	6.67×7.50	31.1	+42	345
Green	60/para	7.00×13.03	43.8	+42	345
Red	20	10.36×12.25	8.2	+42	345
Red	60	10.93×14.06	27.5	+42	345
Blue	20/para	5.41×6.80	-26.0	-42	345
Blue	60/para	5.77×12.86	-36.8	-42	345
Green	20/para	6.58×7.62	-26.5	-42	345
Green	60/para	6.88×13.37	-37.1	-42	345
Red	20	10.42×12.32	-3.5	-42	345
Red	60	11.01×14.50	-23.7	-42	345
Blue	20/para	5.57×6.33	52.9	+63	160
Blue	60/para	5.82×12.09	62.6	+63	160
Green	20/para	6.73×7.29	52.6	+63	160
Green	60/para	6.94×12.65	62.5	+63	160
Red	20	10.53×12.06	9.3	+63	160
Red	60	11.38×13.34	41.5	+63	160

Table 3: Results of fitting 2-dimensional gaussians to the recentered PSF of Vesta for the two parallel mode ‘magic’ scan orientation angles. OD160 results for orientation angle +63 are repeated for completeness.

and simply integrating longer will pose a danger of detecting additional fainter background sources. Figures 5 to 7 present observations of Vesta (using a longer integration than presented above), Neptune and Mars. These will reveal progressively fainter PSF detail or straylight effects compared to the PSF core, but the Mars observations are already fully saturated in the center.

For this reason, scanmaps of Mars (OD137, parallel mode) and Neptune (OD173, scanmap) were inspected only for faint PSF details. Both objects being SSOs without associated nebulosity, they may nevertheless be useful as a reference for other bright source observations. Note that Neptune’s brightest moon Triton may reach about 0.5Jy in the blue but should be in the inner part of the PSF at radius ≤ 15 arcsec.

It should be noted again that some of the features (ghosts, crosstalk) will show up at different levels, depending on which region of the array and of the instrument was crossed by the source in the particular observation, and how exactly the data were reduced. We illustrate this in Figure 8 using the example of the blue Vesta data already shown above. The left panel shows the map from the PSF analysis, using only frames with the source centered within a matrix by some margin, and recentering each frame. The middle panel shows a more normal reduction, using all data and (for illustration) a more relaxed deglitching nsigma. Differences between the two images are: (1) the expected slight global shift of the psf core due to the use of recentering or not. (2) the presence of a negative crosstalk signature in the normal processing, because the frames where the source is centered on crosstalking pixels are included, and because deglitching is relaxed enough to let pass these events. Different deglitching methods and parameters can weaken this feature again. (3) a weak diagonal excess emission related to the ‘blue streak’ ghost feature occuring with the source just outside the corner of the blue array (See FM-ILT report).

Neptune observations confirm the features seen in Vesta. More clearly detected is a dark spot in the +y detection, at a separation differing in blue/green vs red and clearly originating in crosstalk effects (see also PICC-ME-TN-034). Note that the detectability of the spot is a clear function of the deglitching procedure used, like the source itself it may be ‘deglitched away’ if blindly applying parameters suited for faint source

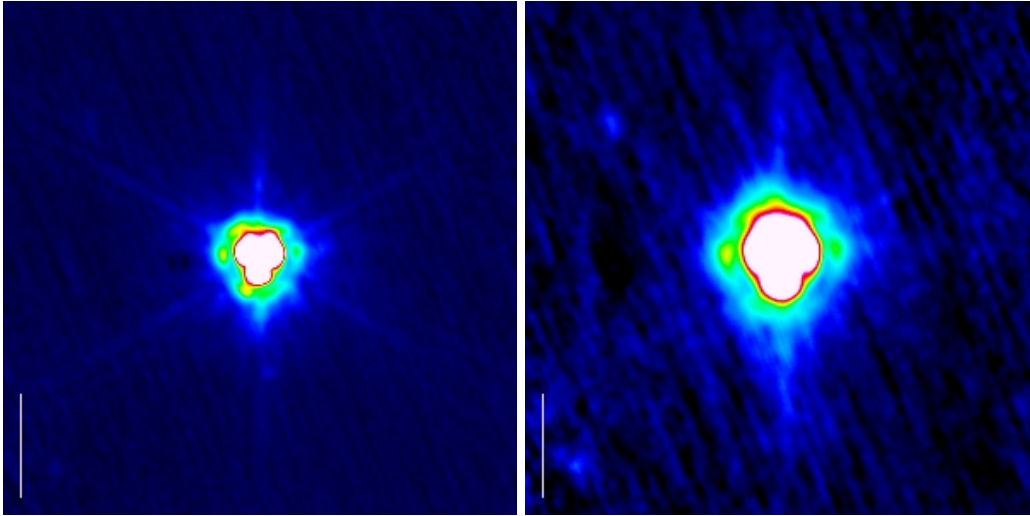


Figure 5: Deep Vesta observations from OD348, left green, right red. Scaling is between -0.0005 and 0.01 of the PSF peak. The dark spots to the left are a crosstalk effect. Comparison to the Neptune observations suggests that the two objects to the top and bottom left may be background objects rather than PSF features.

fields.

Very weakly indicated in the Neptune maps are possible linear structures, elongated in z direction and offset by roughly multiples of matrix sizes n in y direction. Similar features are indicated in the coadditions of many Vesta datasets as well as in certain Key Programme science observations of bright stars. The offsets from the source which are about commensurate with matrix sizes suggest an origin in PACS by a to be identified mechanism.

The maps of Mars clearly show the 60 degree symmetry multi-spoke pattern expected from the secondary mirror support (see also PICC-ME-TN-029). In both bands, an elongated feature crossing the source in scan direction is observed, likely due to an aftereffect of passing this extremely bright object. Both bands show a weakly elevated structure, roughly rectangular in spacecraft y (array) direction, related to the effects discussed in Section 6. The blue map shows clear deglitching artefacts, the red one a crosstalk artefact ~ 1.7 arcmin to the left of the source that is likely further modified by deglitching.

5.3 Comparison to modelled PSFs

After convolution with the PACS pixel size, the modelled PSFs of PICC-ME-TN-029 for the ‘as built’ telescope can be compared to the recentered PSFs of Table 2. For a Rayleigh-Jeans slope SED the models predict a gaussian fit FWHM of 4.7, 6.1, and 9.9 arcsec for blue, green, red with minimal noncircularity. Even the slow speed recentered measured PSFs, where scan related smearing can be ignored, show a roughly 10% larger PSF width and also a clear elongation in red, which are not captured by the Herschel model. This may be due to both inaccuracies of the model adopted in PICC-ME-029 and to effects within PACS. As noted, an elongation of the red PSF was already suggested from ILT testing, indicating that this effect may arise within PACS.

Figure 9 shows the models over an image size and flux scaling directly comparable to the Vesta PSFs from

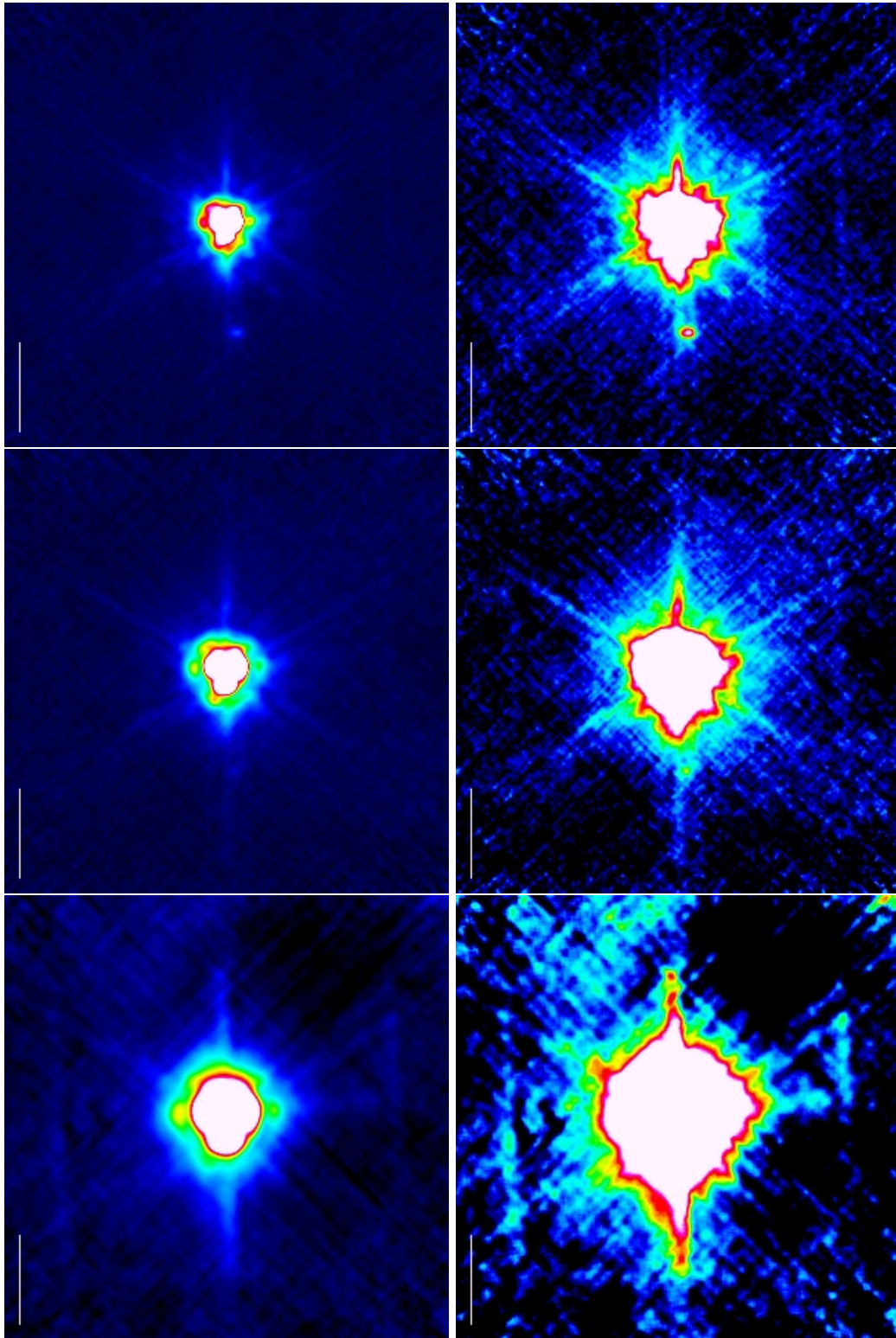


Figure 6: Faint PSF details from scanmaps of Neptune, in blue (top) green (middle) and red (bottom). Maps are averages of two different scan directions 45 and 135 deg. The scale bar indicates 60arcsec. Scaling is between -0.0005 and 0.01 of the PSF peak (left) and -0.00005 and 0.001 of the PSF peak (right).

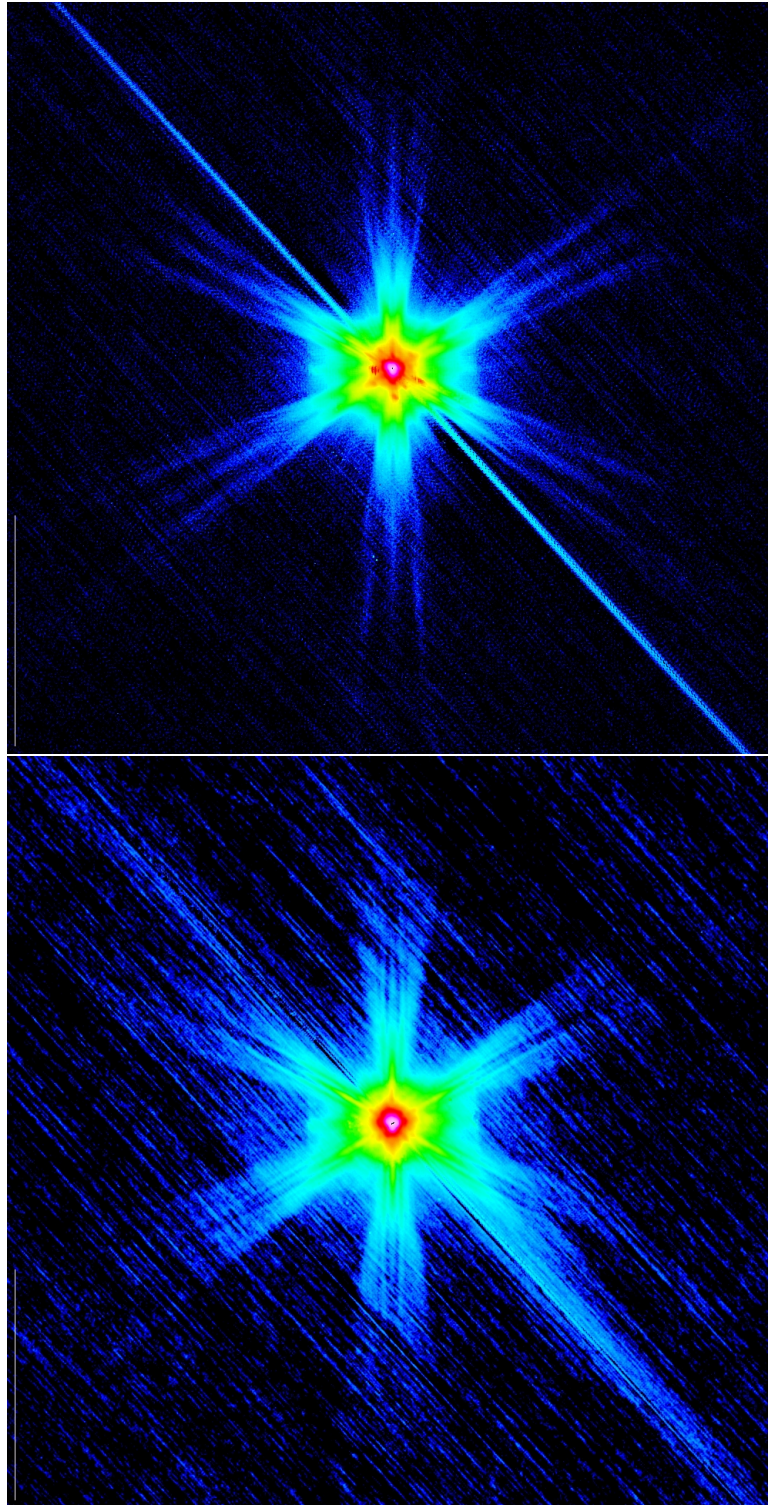


Figure 7: Faint PSF details from scanmaps of Mars, in blue (top) and red (bottom). The scale bar indicates 10 arcmin.

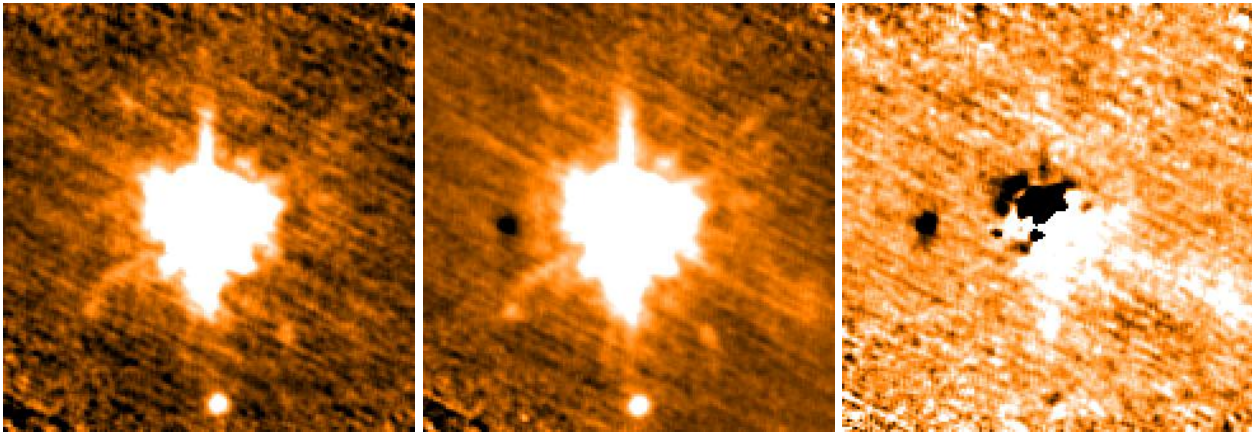


Figure 8: Illustration how mapped area and processing may affect the retrieved PSF. Left: Vesta as processed for the PSF analysis, using recentering. Middle: Normal processing from full AOR and with relaxed deglitching, Right: Difference image.

Figures 1 to 3. The models reproduce well the observed basic morphology, in particular the tri-lobe appearance. As noted, they fail to reproduce the elongated red PSF. They also do not reproduce in detail the relative strengths of the various PSF knots. Going yet fainter, Figure 10 shows outer regions of the blue and red PSF that can be compared to the Mars observations in Fig. 7. The basic sixfold symmetry is well reproduced but there seems to be a tendency for some of the individual rays in the substructure of each of these six branches being more diffuse in the observation. As an example, consider radii of 5-10 arcmin in the blue psf. The finite ~ 6 arcsec size of Mars during the observation may contribute here.

Comparison of the inner few arcmin of the observed (Mars) and modelled PSFs shows a number of discrepancies where the observed PSFs break the six-fold symmetry. One example is the elongation of the observed PSFs in y direction leading to a more rectangular appearance at the level shown in light blue in Fig. 7. Another one is the enhanced flux seen at $PA \sim 240$ deg at radius 1-2arcmin in the blue Mars PSF. We discuss in the next section to which extent they can be explained by ghosts and other PACS peculiarities.

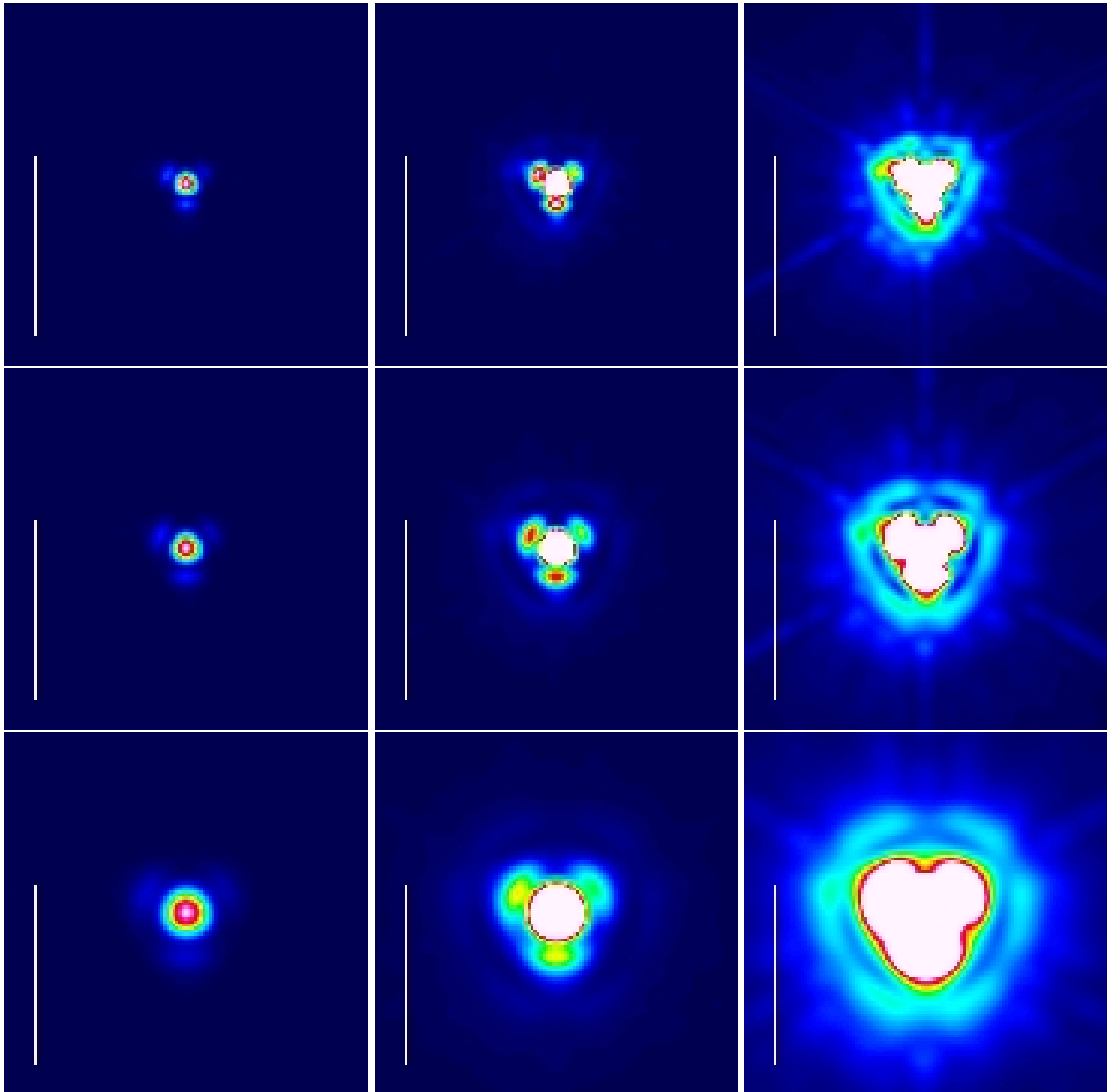


Figure 9: PSF details from model PSFs for a Rayleigh-Jeans source. From left to right linearly scaled to peak, 10%, and 1% of peak. Top: blue, Center: green, Bottom: red. The scale bar indicates 1 arcmin. To be compared to the observed PSFs in the top rows of Figs. 1 to 3.

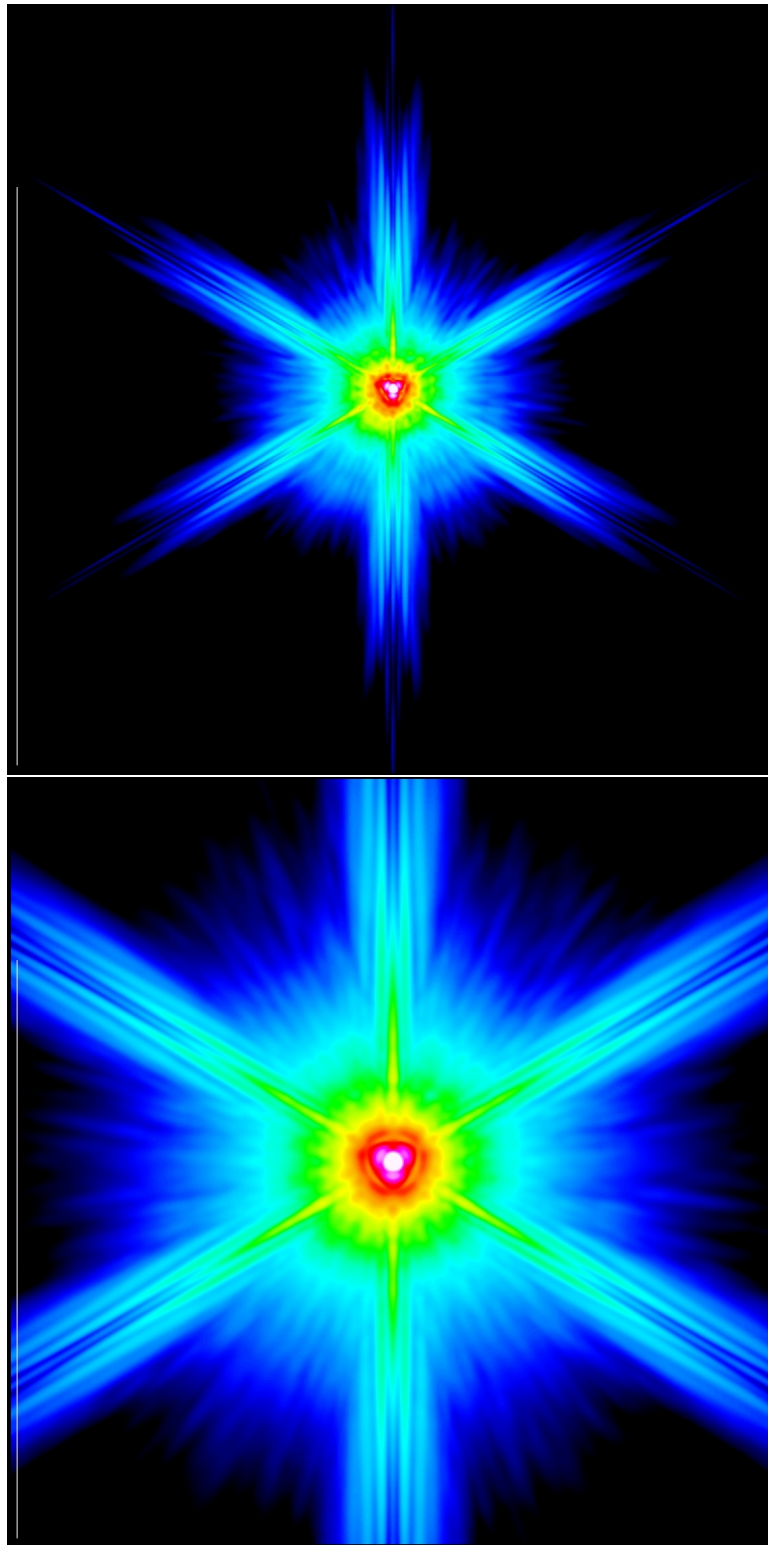


Figure 10: Faint PSF details from model PSFs for a Rayleigh-Jeans source. Logarithmic display. Top: blue, Bottom: red. The scale bar indicates 10 arcmin.

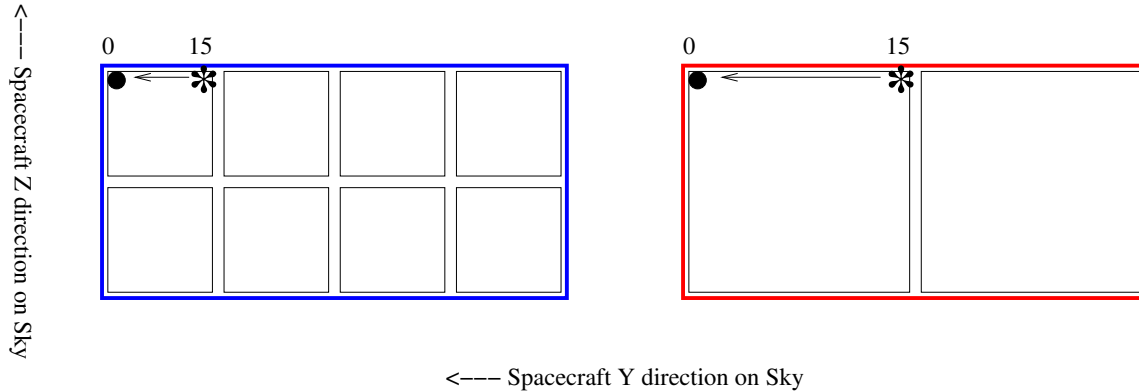


Figure 11: Schematic illustration of crosstalk within the blue and red matrices of PACS. If the source (asterisk) is placed above column 15 of a given matrix, crosstalk effects are seen in the same matrix in column 0 of the same row.

6 Impact of saturation, crosstalk, ghosts and straylight on observed PSF

6.1 Saturation aftereffects

For the observations of Mars, the pixels centered on the source are heavily saturated. While the detector comes out of saturation quickly it does not recover instantaneously to the pre-saturation signal. This leads to significant trails in scan direction for the highpass filtered maps shown in Figure 7. See also the saturation aftereffects in the panels of Fig. 17, showing cuts through the arrays as function of time. Because these effects are quite variable in magnitude and sign from pixel to pixel, they interact in a complex way with the mapping and 2nd level deglitching.

6.2 Detector crosstalk

An electrical crosstalk is observed in the PACS arrays between columns 15 and 0 in the same row within each matrix (see sketch in Fig. 11). The amount of crosstalk depends on the setup of the bolometer control voltages and nonlinearly on source flux (K. Okumura, priv. comm.). For a bright source (V814 Her) and the in-orbit bolometer settings, crosstalk signal in column 0 was typically a few percent of the true signal in column 15 and negative (PICC-ME-TN034). Some red pixels show strong positive crosstalk and are thus excluded by the current bad pixel mask.

Crosstalk will hence induce a negative image that is offset by about 50 arcsec (blue, green) and 100 arcsec (red) towards positive spacecraft Y direction. Its magnitude in a final map will vary, depending on how often the source crossed column 15 (see Fig. 8 for illustration), and on the deglitching methods used which will tend to decrease the magnitude of the effect.

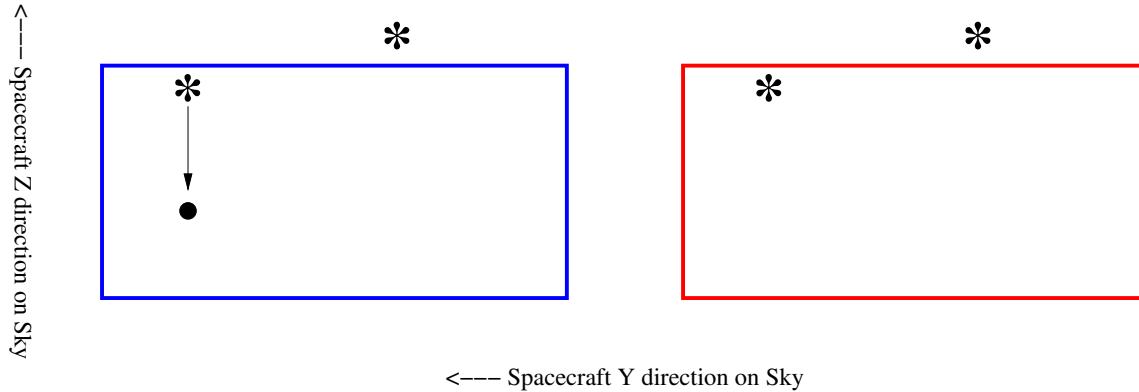


Figure 12: Schematic representation of the compact ghost image seen in blue if a bright source (asterisk) is placed on the array. No ghost is seen with the source off the array. No effect of this magnitude is observed for the red.

The crosstalk signatures are visible in various figures of this note, in our PA=0 visualisations they are found offset to the left from the source peak.

In datasets where this is possible in terms of S/N and redundancy of the adopted scanning scheme, the crosstalk effect on the PSF can be suppressed by excluding the first column of each detector matrix from the analysis. This can be done by declaring columns 0, 16, 32, 48 for blue and 0, 16 for red ‘bad’ in the bad pixel calfile.

6.3 Ghosts in blue array

Section 5.1 noted the presence of a compact blue/green PSF feature offset about 70arcsec in negative z direction from the PSF peak. Inspection of the Mars data frame by frame shows that this feature is present only if the source itself falls on the array, but not if it has moved off in z direction by a small amount that would still keep the feature on the array (Figs. 12 and 13). This clearly argues for an origin in PACS rather than the Herschel telescope.

An electrical crosstalk effect would in principle be consistent with this behaviour. We consider it an unlikely explanation, however, because the crosstalk effect would have to occur between different rows of different matrices, and because the different ratio of feature to PSF peak for blue and green (Fig. 6) would need additional nonlinearity as an explanation.

We interpret the feature as an optical ghost, offset from the PSF peak by about -70arcsec in z and -7arcsec in y and reaching about 10^{-3} of the PSF peak in blue and 5×10^{-4} in green. No such feature was observed in red. Since the feature will be present only in part of the data, its magnitude can in principle be affected by 2nd level deglitching if the source is extremely bright.

A weaker ghost feature is observed in the blue if a very bright late type star is just at the corner of matrix 4 (Figs. 14 and 15). It is well possible that similar or weaker ghosts occur for yet other source positions and

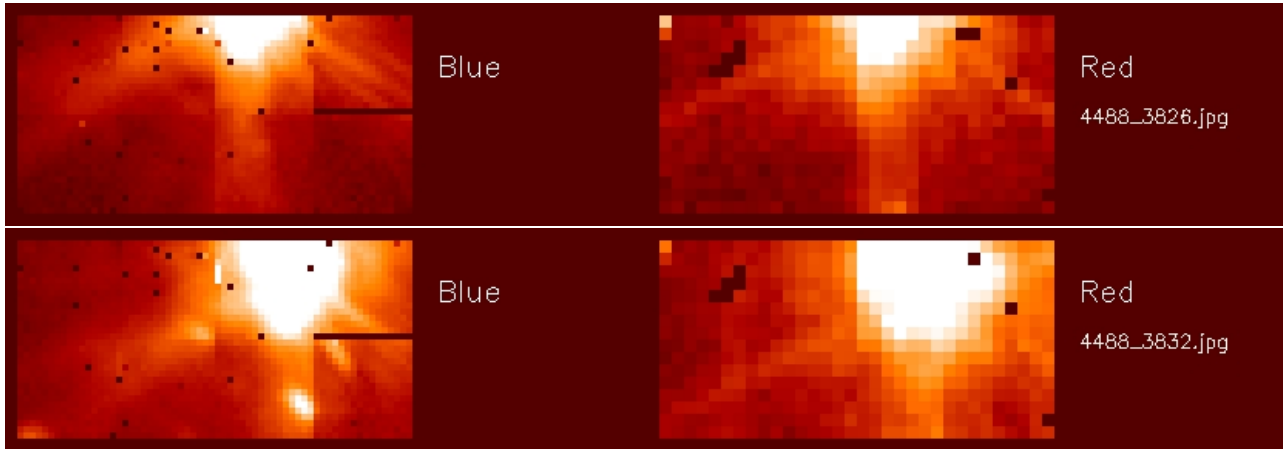


Figure 13: A ghost image on the blue array, shifted about 70arcsec in negative z direction from the true source, is invisible while the source is just outside the array (top) but visible with the source on array (bottom). No such feature is seen in red. Note the weaker features that also don't move with the source, suggesting these are ghosts.

contribute to some of the weak knots in integrated PSFs. Future finer mapping of the focal plane with such very bright sources will better characterise the incidence.

6.4 Blue streaks, other reflections and straylight effects

A number of peculiar effects are observed while very bright sources are just outside the limits of the array(s). For some of them the morphology clearly suggests an origin in reflections/ghosts off the PACS structure, in other cases direct optical as well as other explanations appear possible.

The brightest of these phenomena are the diagonal 'blue streaks' already observed during ILT, with point sources just outside the blue array corners. They are strongest for the top left corner (Figs. 16 and 17). During the peak of the event these can reach up to about 4% of the source peak (PACS FM-ILT report). In a real map this will be diluted by other PACS pixels having seen the same spot on the sky without being affected. The amount of this dilution will be a function of AOR layout and specific source position. Second level deglitching may change the result further. For the Mars blue map (Fig. 7) the streak is clearly seen but finally at the 10^{-3} level, and obviously affected by deglitching.

Similar but less pronounced effects have been observed with sources at the edges of the red array, producing linear streaks that extend in vertical or (weaker) horizontal direction (Fig. 18). Inspection of neighbouring red frames as well as of the blue channel shows these again are localized effects rather than general PSF features. The vertical feature in Figure 18 reaches maximal intensity (at a location close to the opposite array edge) of about 1% of the PSF peak, the weaker horizontal one stays around the 10^{-3} level. Both numbers refer to the individual most affected frame.

It is possible that these features contribute to the linear PSF feature in vertical (z) direction (Sect 5.1) that aligns with one of the six diffraction spokes caused by the secondary support, but is too strong in comparison to the other spokes. No full mapping of a super-bright source is available which would be able to test whether

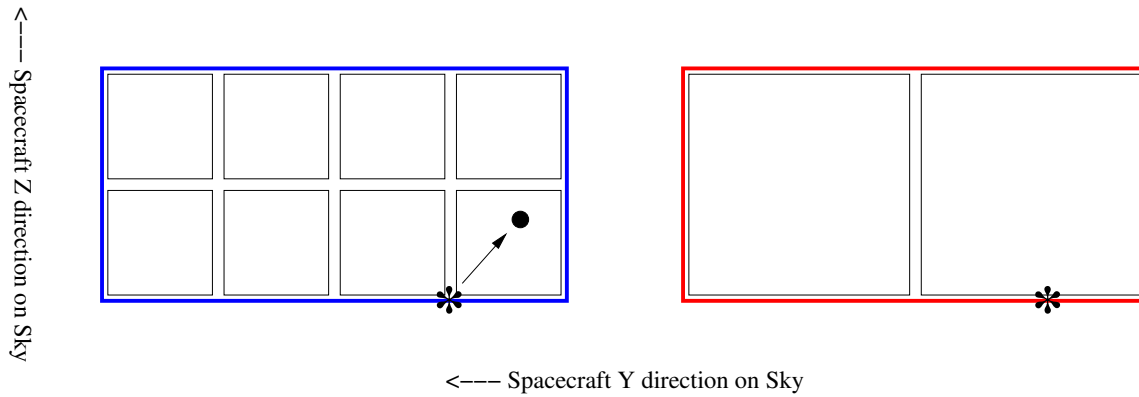


Figure 14: Schematic representation of the compact ghost image seen in blue if a bright source (asterisk) is placed on the corner of matrix 4. No effect of this magnitude is observed for the red. Current data and analysis neither confirm nor exclude similar effects in other matrices.

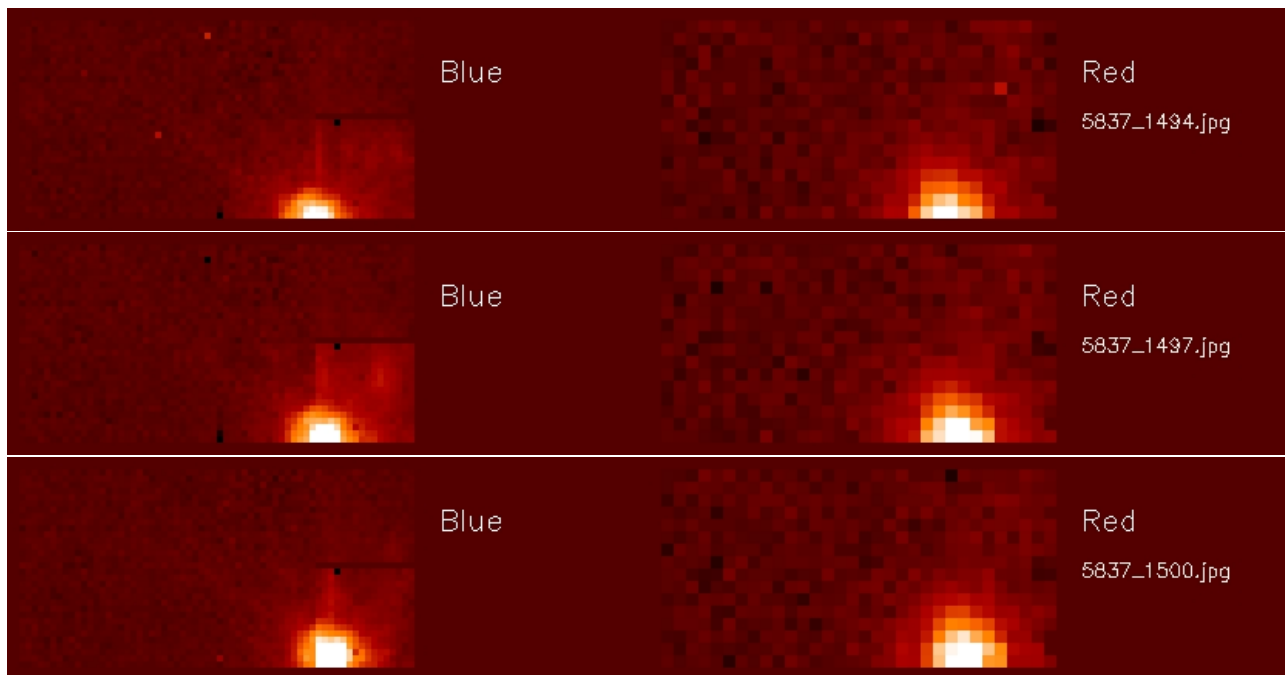


Figure 15: A ghost image on the blue array, shifted about 50arcsec diagonally from the true source across matrix 4 is visible in the middle panel of this sequence. No such feature is seen in red.

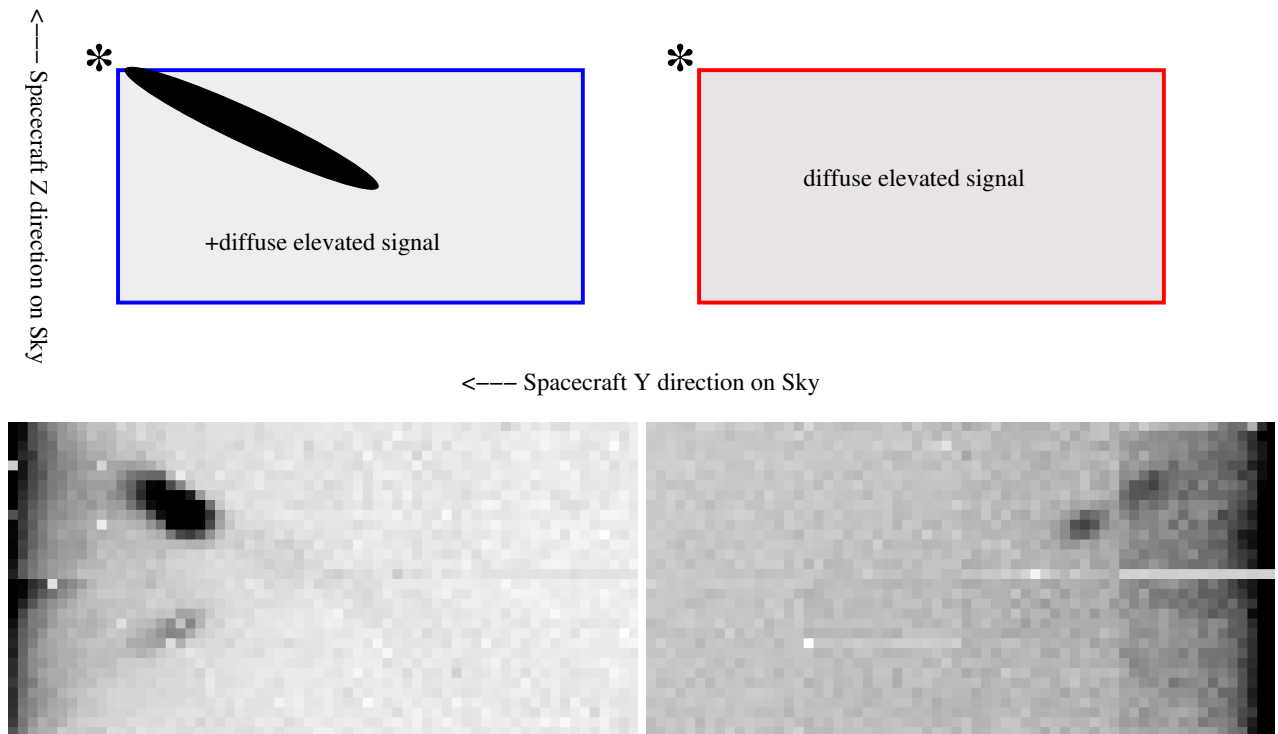


Figure 16: Top: With a bright source placed just outside the top left corner of the blue array, a diagonal ‘blue streak’ is crossing the array. At the same time, there is a generally elevated signal in blue and in particular red. Bottom: Similar but weaker streaks are seen with sources outside the other corners of the blue array. The two panels show ILT results using the extended PACS internal calibration source just outside the blue field of view.

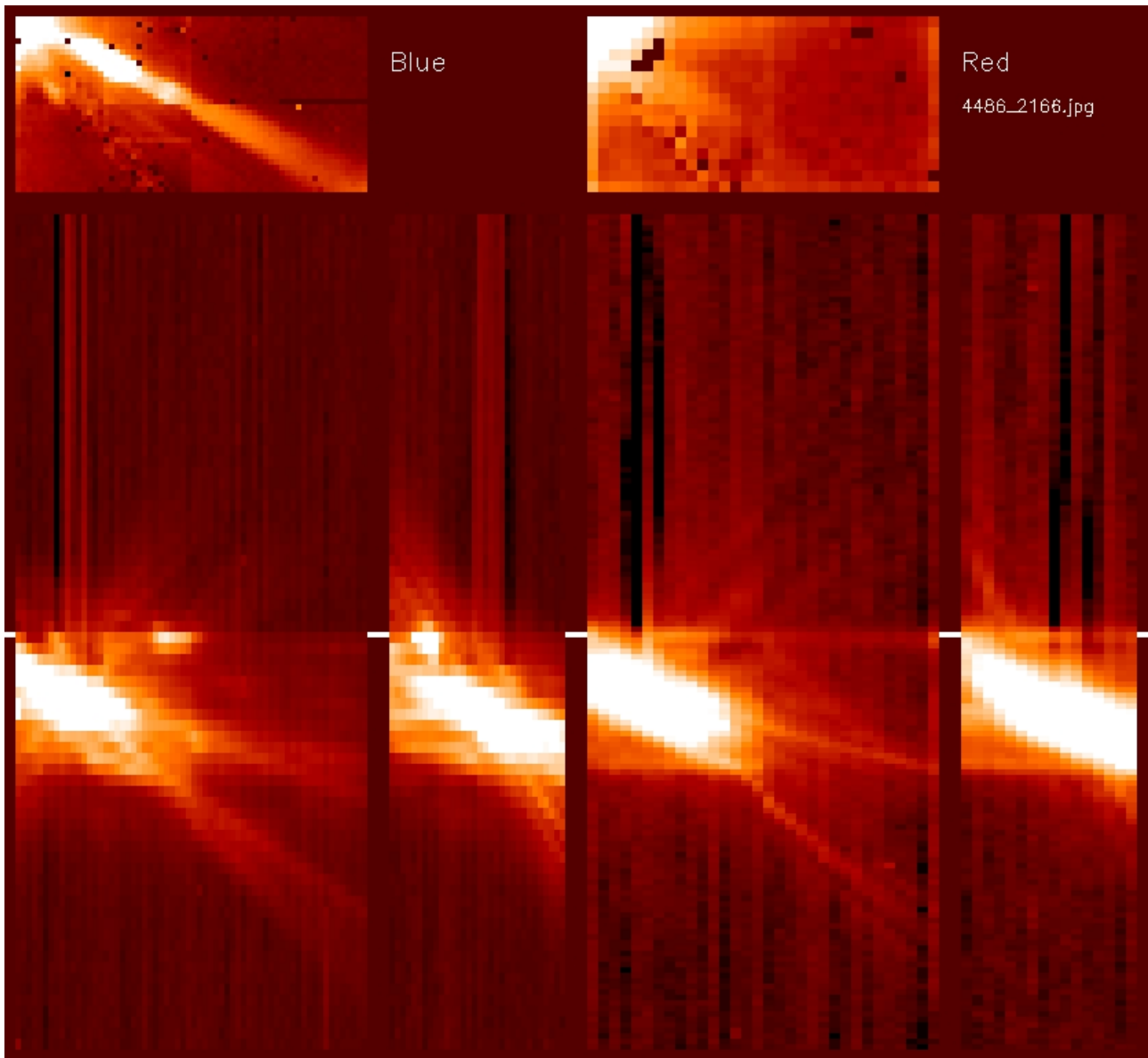


Figure 17: Diagonal streak in the blue array, with Mars just outside the top left corner. At the same time the signal in red array is generally elevated. The bottom panels show cuts through pixel 14,14 of the blue array and 7,7 of the red array, as a function of time rising upwards.

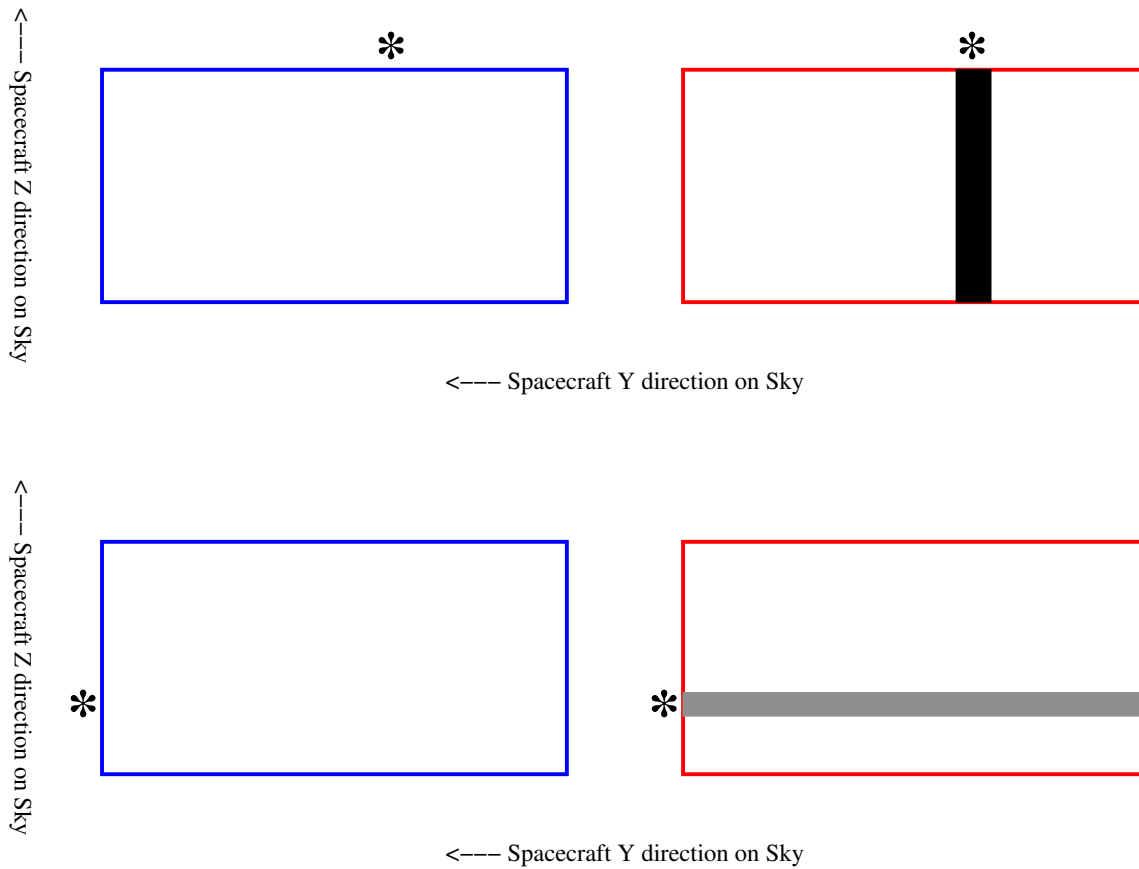
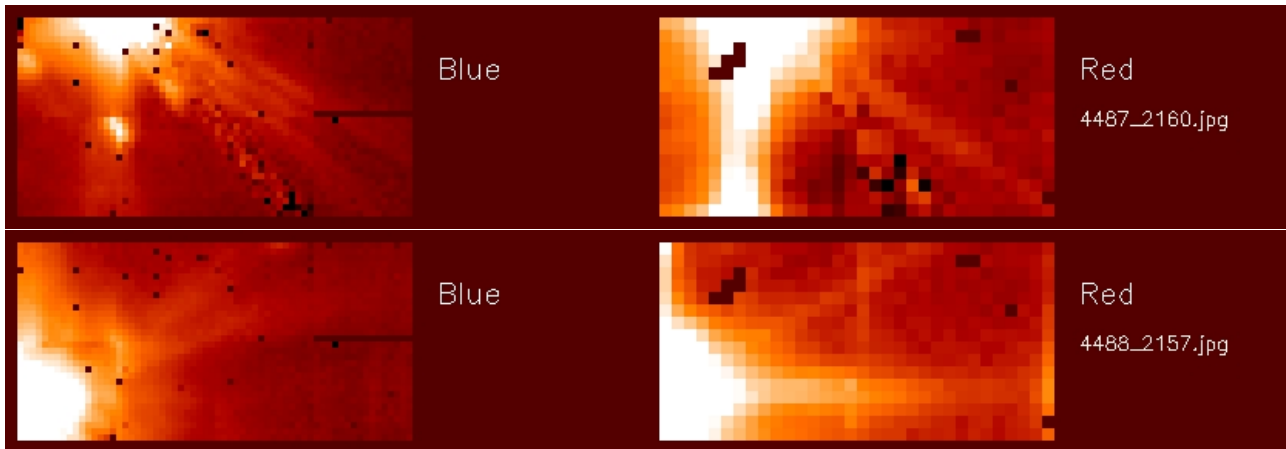


Figure 18: Red streaks. Top: vertical reflection with the source just off the upper array edge. Bottom: horizontal reflection with the source just off the left array edge.

the phenomenon occurs along the full edges of the red array or just small parts. Such a mapping may also help verifying whether the shorter and more asymmetric linear feature seen in blue has a similar origin. This is plausible but not yet demonstrated from the data and analysis in hand.

6.5 Implications of peculiar effects

The reflections, ghosts, and crosstalk effects presented here are very faint relative to the source and will be irrelevant for most science cases. Their total effect on the encircled energy is implicitly captured in the EEF curves derived below.

They may however need explicit consideration for a subclass of observations trying to detect very faint sources or structures near very bright sources, with a dynamic range above $\sim 10^3$. Given that the effects strongly depend on the path of the source crossing the array, it may be advisable to supplement the source observations inside the program with an explicit PSF standard observation taken with *exactly* same AOR layout in array coordinates.

7 Effects of data reduction methods and of source SED

7.1 Effects of highpass filtering

If using the masking and highpassfiltering reduction scheme with small filtering radii to boost point source sensitivity, the wings of the PSF will be obviously reduced. Since details will depend on the adopted parameters and source properties, no quantitative results are provided here.

7.2 Standard data reduction vs. recentering

Band	Speed arcsec/sec	FWHM arcsec α Tau OD118 normal processing	PA deg	FWHM arcsec α Tau OD118 recentered	PA deg	Ratio
Blue	10	5.46×5.78		5.20×5.56		1.045
Blue	20	5.60×6.27		5.40×5.70		1.068
Blue	60	5.92×9.17	61.0	5.70×8.92	61.6	1.033
Green	10	6.68×6.95		6.52×6.76		1.026
Green	20	6.77×7.29		6.63×6.83		1.044
Green	60	7.02×9.92	61.9	6.84×9.66	61.8	1.027
Red	10	10.59×12.08	10.6	10.41×11.98	8.1	1.013
Red	20	10.89×12.24	15.3	10.58×12.06	9.4	1.022
Red	60	11.34×13.37	39.5	11.35×13.30	40.8	1.002

Table 4: Comparison of PSF widths for normal and recentered processing. Results of fitting 2-dimensional gaussians to the α Tau PSFs. Ratio is the ratio of circularized PSF widths. *Scan orientation angle is 63deg for these observations.*

The recentering procedure, if applied, implicitly corrects for satellite pointing jitter, residual timing shifts satellite vs. instrument data, and inaccuracies of the spatial calibration, in particular the ArrayInstrument calfile. To give an example for the order of magnitude of the effect, we have reduced the same OD118 α Tau data once with a normal script and then with recentering. Table 4 summarizes the results and the ratio of circularized PSF widths, $\text{Ratio} = \sqrt{\text{FWHM}_a \times \text{FWHM}_b_{\text{Normal}}} / \sqrt{\text{FWHM}_a \times \text{FWHM}_b_{\text{Recentered}}}$.

For these particular observations the increase of PSF width in normal processing is typically a few % but is expected to be a function of, e.g., pointing quality during a particular observation.

7.3 Effects of source SED

Because of the large spectral width of the PACS filters, noticeable effects of SED slope on PSF width are expected. We verify this by dedicated observations of the Blazar 3C345 in comparison to the α Tau data. Both are fixed targets and observed with same AOR setup. No recentering was applied due to the faintness of 3C345, which also prevents analysis beyond the determination of PSF width (Fig. 20). Table 5 shows a PSF width that is on average lower by a few % for α Tau compared to 3C345, with scatter due to the weakness of 3C345.

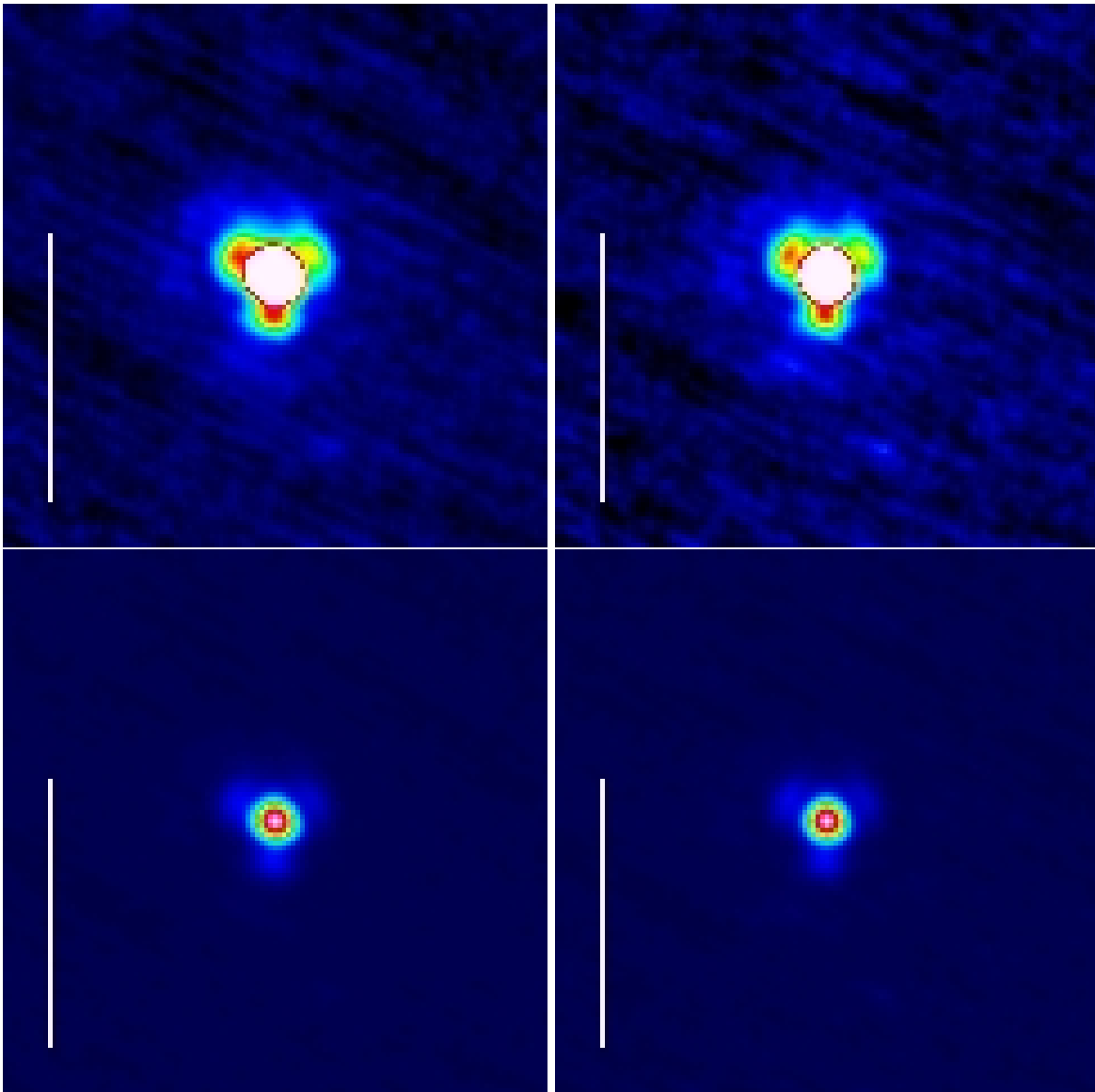


Figure 19: Slight sharpening effect of recentering on the PSF. The same green 20 arcsec/sec α Tau observation is shown on the left with normal processing and on the right recentered. Top and bottom are different display cuts.

Band	Speed arcsec/sec	FWHM arcsec		PA deg	FWHM arcsec		PA deg	Ratio
		α Tau OD118 normal processing	3C345 OD124 normal processing					
Blue	10	5.46×5.78			5.56×6.05			0.968
Blue	20	5.60×6.27			5.76×6.16			0.995
Blue	60	5.92×9.17		61.0	5.64×10.75		65.8	0.946
Green	10	6.68×6.95			6.90×7.33			0.958
Green	20	6.77×7.29			6.86×7.42			0.985
Green	60	7.02×9.92		61.9	7.06×11.44		65.4	0.929
Red	10	10.59×12.08		10.6	11.02×12.56		10.9	0.961
Red	20	10.89×12.24		15.3	10.73×12.36		12.8	1.002
Red	60	11.34×13.37		39.5	11.99×15.24		50.0	0.911

Table 5: Comparison of PSF widths for α Tau (blue Rayleigh-Jeans source) and 3C345 (red continuum). Ratio is the ratio of circularized PSF widths. *Scan orientation angle is 63deg for these observations.*

We can compare these results to expectations from the modelled ‘as built’ Herschel PSF of PICC-ME-TN-029, after convolution with the PACS pixel size for f_λ SED slope of -4 (roughly matching α Tau) and -1 (roughly matching 3C345). We derive for the model PSFs circularized FWHM ratios of 0.979, 0.971, and 0.956 which are consistent with Table 5 given the S/N of the 3C345 data, and the presence of PSF effects that are not covered by the model.

7.4 Effects of drizzling

Band	Speed arcsec/sec	FWHM arcsec		PA deg	FWHM arcsec		PA deg	Ratio
		Vesta OD160 no drizzle	Vesta OD160 drizzle					
Blue	10	5.25×5.61			4.84×5.18			1.084
Green	10	6.53×6.78			6.24×6.49			1.046
Red	10	10.38×11.95		6.3	9.54×11.14		6.6	1.080

Table 6: Example of the effect of drizzling on the PSF width, comparing results of a Vesta recentered reduction with standard PhotProject with a drizzled reduction with pixfrac ~ 0.15 .

By default, PACS maps created with the PhotProject tool assume in projection an active pixel size of $640\mu\text{m}$ within the pixel pitch of $750\mu\text{m}$. This ‘Okumura-Gastaud constant’ is guided by the physical structure of the bolometer pixels and the inter-pixel walls. ‘Drizzling’ by projecting with smaller pixels can reduce the noise correlation between neighbouring map pixels and also sharpen the PSF. A pixfrac parameter is hence being introduced in upcoming versions of PhotProject.

Figure 21 and Table 6 present an example showing that such drizzling can influence the PSF width at the 5% to 8% level. The effect is smallest in green where the PSF width is already better sampled by the natural PACS pixel size.

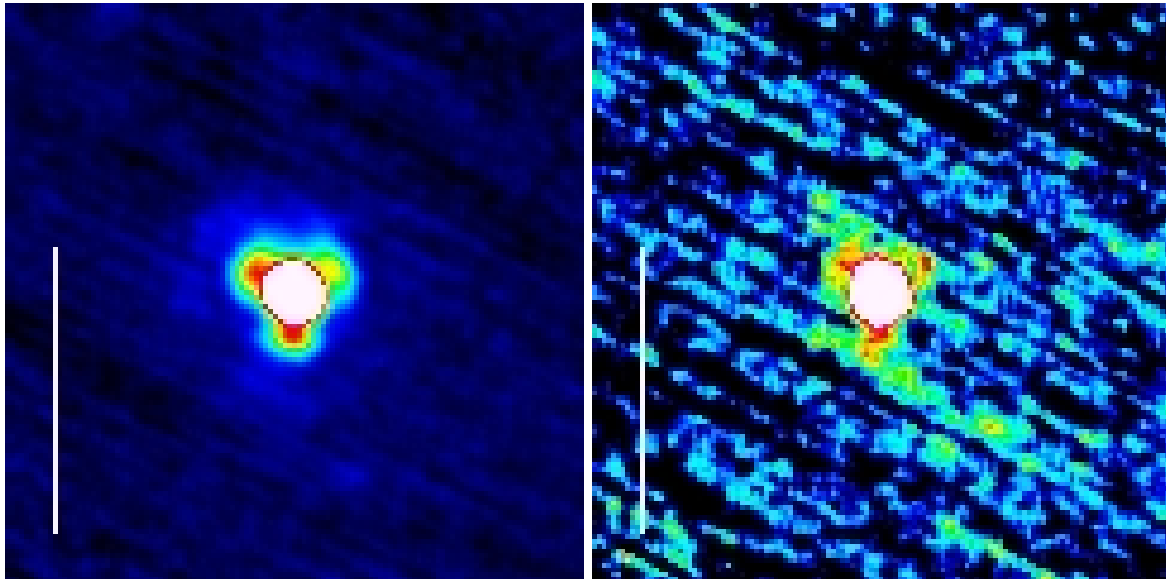


Figure 20: Example of observation to verify the effect of SED slope on PSF width. Left is a green $20/\text{arcsec}/\text{sec}$ αTau with normal processing, right the equivalent observation for 3C345. Given flux and S/N of 3C345, comparison is limited to PSF width confirming the expected increase for a red source.

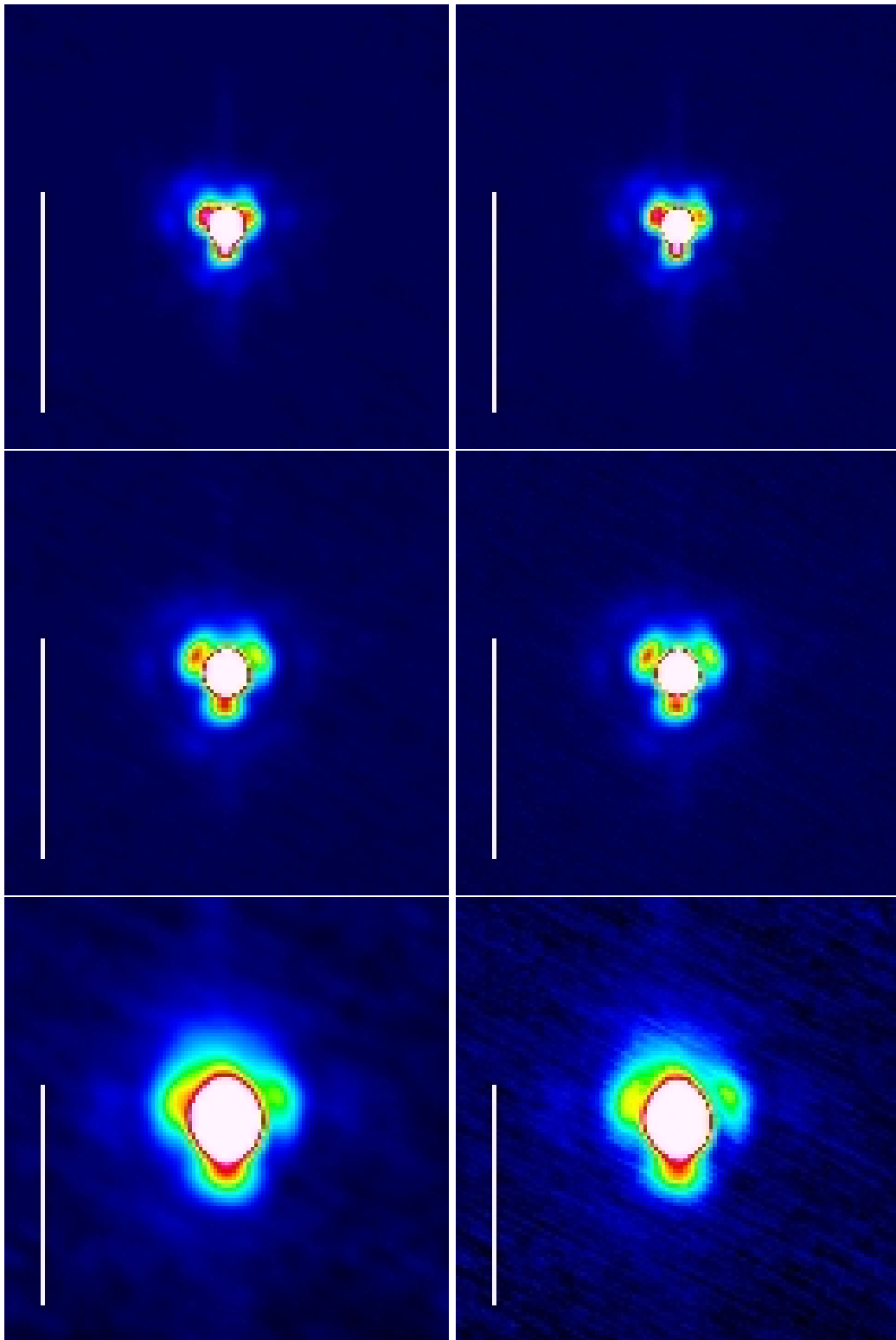


Figure 21: Sharpening effect of drizzling on the PSF for the same Vesta 10arcsec/sec observations, blue-green-red from top to bottom. Left: recentered, standard PhotProject. Right: recentered, drizzled with 750/8 μ m pixel size (pixfrac \sim 0.15).

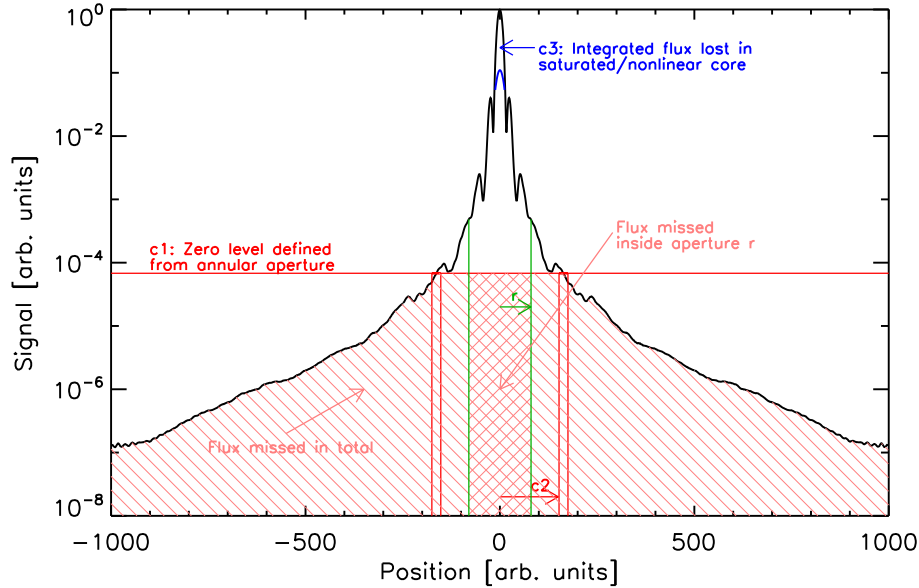


Figure 22: Schematic representation of effects on the measured encircled energy fraction. The ideal EEF would divide the integral of the true PSF (black) inside an aperture r (green) by the integral to infinity. For the ‘observed’ EEF the background subtraction, setting to 0 the flux in an annulus outside radius $c2$, will cause flux to be missed both within the aperture and from the total which is also cut at $c2$. Additionally flux $c3$ may be lost in the PSF core due to nonlinearity or saturation.

8 Encircled energy diagrams

‘Encircled energy fractions’ for various aperture sizes are a key quantity in homogenizing point source photometry obtained with different methods or aperture sizes, and in establishing the extended source calibration of PACS. Practical limitations in its determination arise from S/N, limited dynamical range and saturation, and from the reduction methods described above. This is qualitatively illustrated in Fig. 22.

We adopt the definition

$$EEF(r) = \frac{\int_0^r \int_0^{2\pi} PSF(r, \phi) dr d\phi}{\int_0^\infty \int_0^{2\pi} PSF(r, \phi) dr d\phi}$$

but note that several factors limit evaluation of the total integral to a sufficient \sim percent accuracy. (1) Observations of bright but clearly unsaturated sources like Vesta run out of S/N at large radii. (2) The scheme of subtracting background in an annular aperture reduces the PSF at all radii by the average value within that annulus. Note that skipping this step would simply replace it with a less well defined equivalent subtraction, due to the masked highpass filtering. (3) For the brightest sources like Mars, signal will be missing in the PSF core due to nonlinearity and/or saturation. Fig. 22 gives a cartoon representation of these factors.

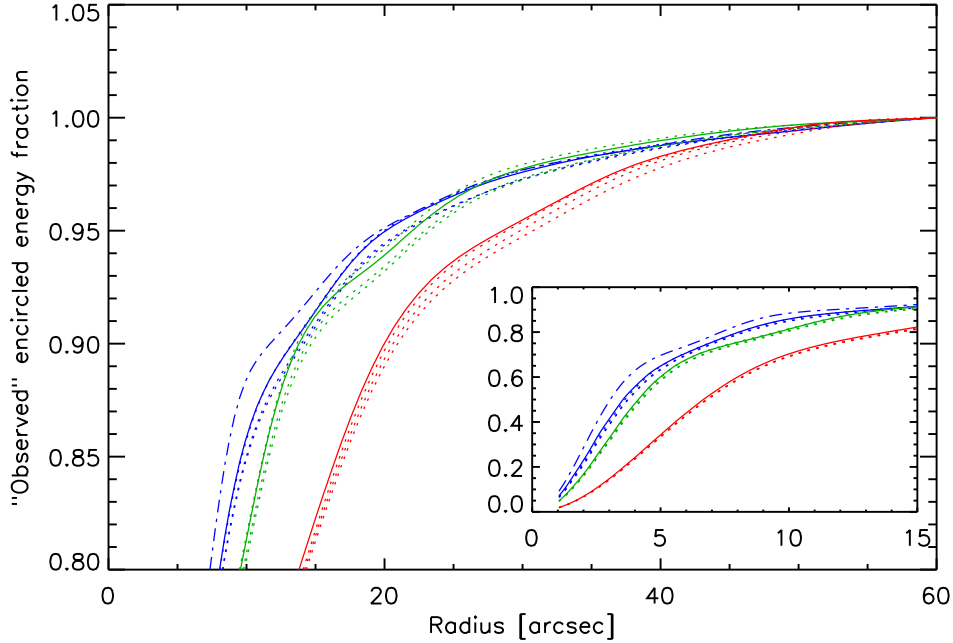


Figure 23: ‘Observed’ encircled energy fraction as a function of circular aperture radius for the three bands. Derived from slow scan (continuous line) and medium speed scan (dashed lines) OD160 and OD345 Vesta data. The EEf fraction shown is normalized to the signal in aperture radius 60arcsec, with background subtraction done in an annulus between radius 61 and 70 arcsec. For blue only, we add with a dot-dashed line the model expectation.

Effectively we are thus using the HIPE annularSkyAperturePhotometry function to obtain from an observation an ‘observed’ EEf that is related to the true PSF like

$$EEF_{obs}(r) = \frac{\int_0^r \int_0^{2\pi} (PSF(r, \phi) - c1) drd\phi - c3}{\int_0^{c2} \int_0^{2\pi} (PSF(r, \phi) - c1) drd\phi - c3}$$

where $c1$ is the average of the true PSF in the annulus used for sky subtraction, $c2$ the radius of the aperture to which the ‘total’ PSF was actually integrated, and $c3$ the flux missing in the PSF core due to saturation/nonlinearity, assuming that both r and $c2$ reach beyond this core. Note that the total PSF integral is too low not only via $c1$ and potentially $c3$ but also by lacking the outer PSF part $\int_{c2}^{\infty} \int_0^{2\pi} PSF(r, \phi) drd\phi$.

8.1 Ancillary information

We are first presenting raw ‘observed’ EEfs of this type from observations and from modelling before attempting to estimate the true EEf.

The PSFs derived from the OD160 and OD345 Vesta data are of sufficient S/N to derive observed encircled energy fractions for the 3 bands as a function of the radius of a circular aperture (Fig. 23). The EEf fraction

shown is normalized to the signal in aperture radius $c_2=60\text{arcsec}$, with background subtraction done in an annulus between radius 61 and 70 arcsec. The agreement between the four measurements at two different scanspeeds is very satisfactory at these large radii, supporting the quality of the data.

A radius c_2 of 60arcsec will miss a nonnegligible part of the PACS PSF. Both modelled PSFs (PICC-ME-TN-029) or large field observations of a super-bright source like Mars could be used to determine this missing flux. The Mars observations could in principle be of limited use if dominated by the saturation aftereffects that are observed in the map. From the comparison of the EEF for the full PSF and just the cleanest quadrant (Fig. 24) its use appears safe, however.

Figure 25 compares the EEF from the model PSFs to the EEF from the Mars result, first uncorrected and then corrected for the Mars flux c_3 lost due to saturation. Both are consistently processed to an observed EEF out to $c_2=400\text{arcsec}$. It appears that the real PSF has more energy at radii above 60arcsec , but only at an excess level $\sim 3\%$ above the model. This excess likely relates to the different anomalous and ghost effects in PACS that were discussed above, which are not included in the model PSF. As a consequence, extrapolation of the Vesta PSFs to larger radii should be done with observed data rather than with telescope PSF models.

8.2 Derivation of EEF curves

Based on these considerations, we derive EEF curves out to 1000 arcsec from the combination of Vesta and Mars data. In this process, the main steps and assumptions are:

- Mars EEF curves for blue and red are derived out to $c_2=1000\text{arcsec}$ where the OD137 Mars maps run out of visible signal. Any flux outside this radius is ignored. The central region of these EEF curves is affected by flux lost due to saturation and nonlinearity, and smeared due to the nonnegligible angular diameter of Mars during the observation (about 6arcsec). No such data are available for green.
- The flux c_3 lost in the central region of the Mars map can be determined comparing the map integral to the nominal Mars flux at the time of observation. The EEF curve is corrected, placing this flux at $r=0$. The resulting EEF is still incorrect at small radii.
- For each band, all Vesta PSFs from OD160 and OD345 taken with speed 10 or 20 arcsec/sec are averaged and ‘observed’ EEF curves out to $c_2=60\text{arcsec}$ derived. No recentering was applied to be representative for a typical reduction.
- From the Mars EEF, the constants c_1 applicable to the Vesta maps are derived.
- The Vesta EEF is corrected for the flux lost due to the nonzero c_1 and the flux outside radius c_2 .
- The two corrected EEFs are overplotted. The factor for the flux lost in the Vesta processing is iterated until the EEF curves visually match at radii approaching 60arcsec . Deviations at smaller radii are expected due to the saturation/smearing effects on the Mars data.

No such procedure can be applied to the green Vesta data, since no green Mars data are currently available. Here we simply adopt averages between the blue and red c_1 constants and the losses at large radii, to correct the green Vesta PSF out to 60arcsec .

Figs. 26 to 28 show the resulting encircled energy fraction curves out to 1000 arcsec , separately for each band and including the contributing Mars and Vesta data. Fig. 29 displays the final combinations for all three bands.

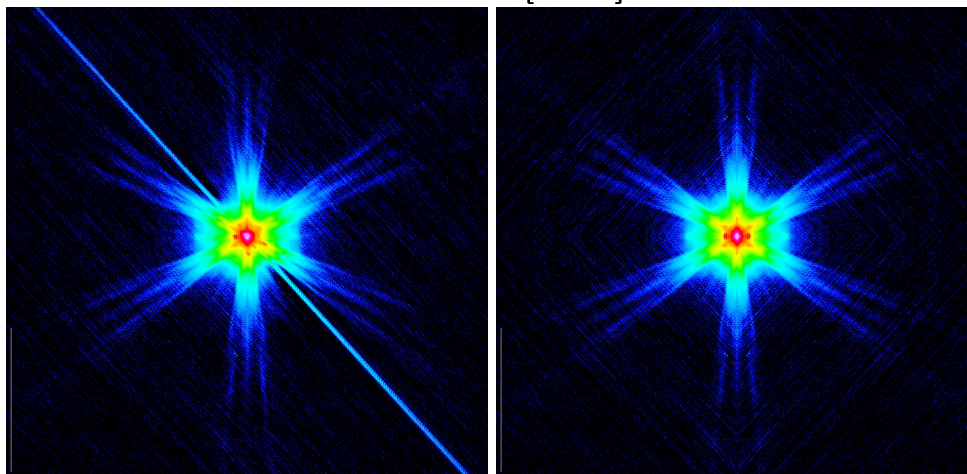
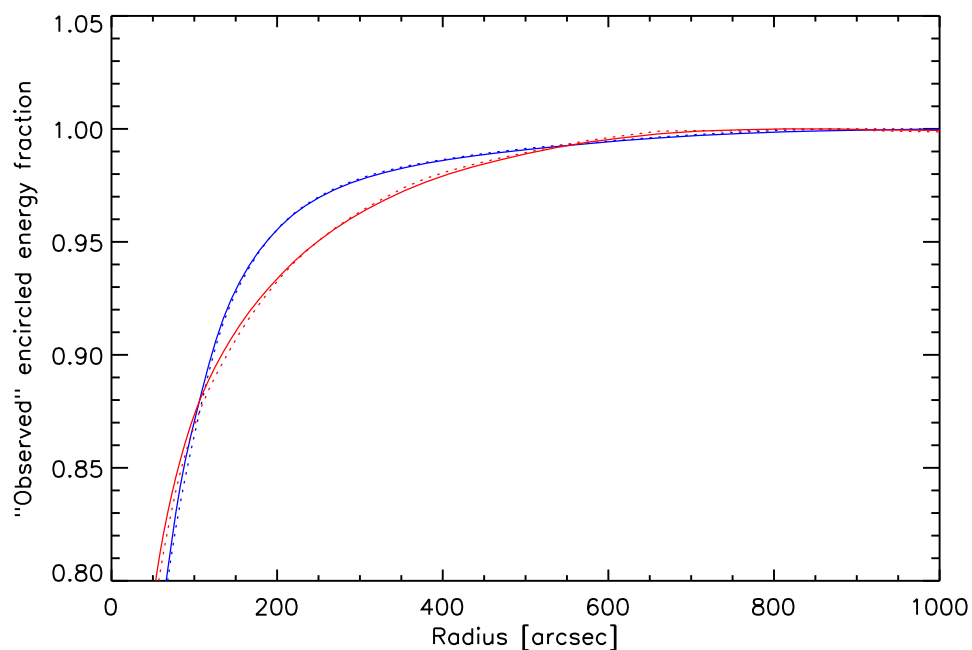


Figure 24: Top: ‘Observed’ encircled energy fraction as a function of circular aperture radius for the blue and red Mars OD137 observation. The EEF from the full map (continuous, see also bottom left) and from the lower left quadrant only (dashed, see also bottom right) agree well, confirming that saturation aftereffects do not dominate the result.

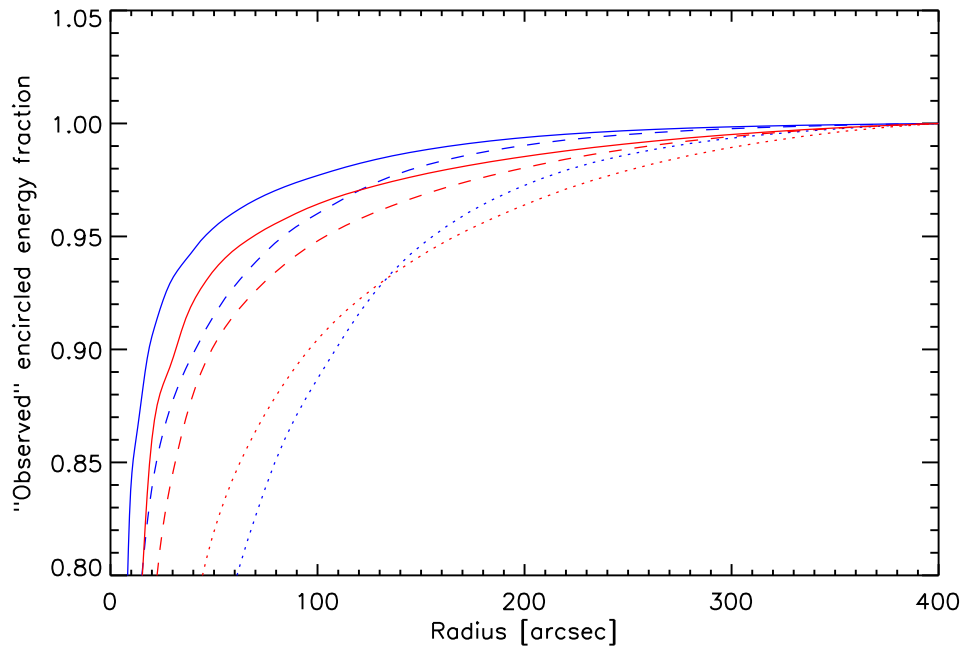


Figure 25: ‘Observed’ encircled energy fraction as a function of circular aperture radius for the blue and red models (continuous), the Mars OD137 data (dotted) uncorrected for saturation, and the Mars OD137 data corrected for saturation (dashed). The observed PSF has more energy at large radii than the model.

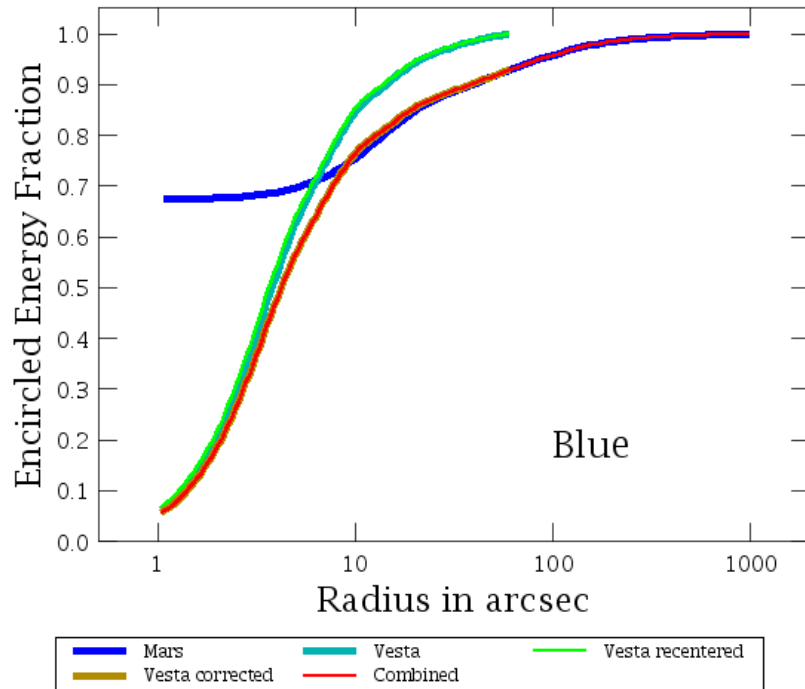


Figure 26: Encircled Energy Fraction for blue. Contributing Mars and Vesta data are shown along with the final combination.

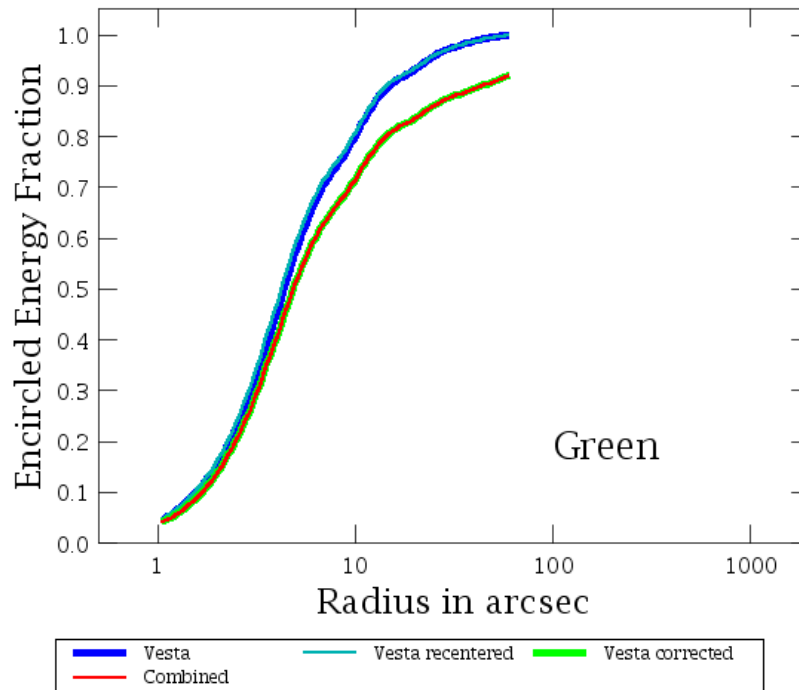


Figure 27: Encircled Energy Fraction for green. Contributing Mars and Vesta data are shown along with the final combination.

We note that the flux in the combined encircled energy curves outside $r=60$ arcsec is 7%, 8%, and 9% in blue, green, and red. In the Vesta processing, the fraction of flux missing combining this loss at large radii with the oversubtraction in the inner region is 9.6% (blue) and 11.7% (red). Recall that the effect of ghosts and other peculiar effects at large radii, estimated above to be a few %, will vary with detailed AOR layout and source crossing path.

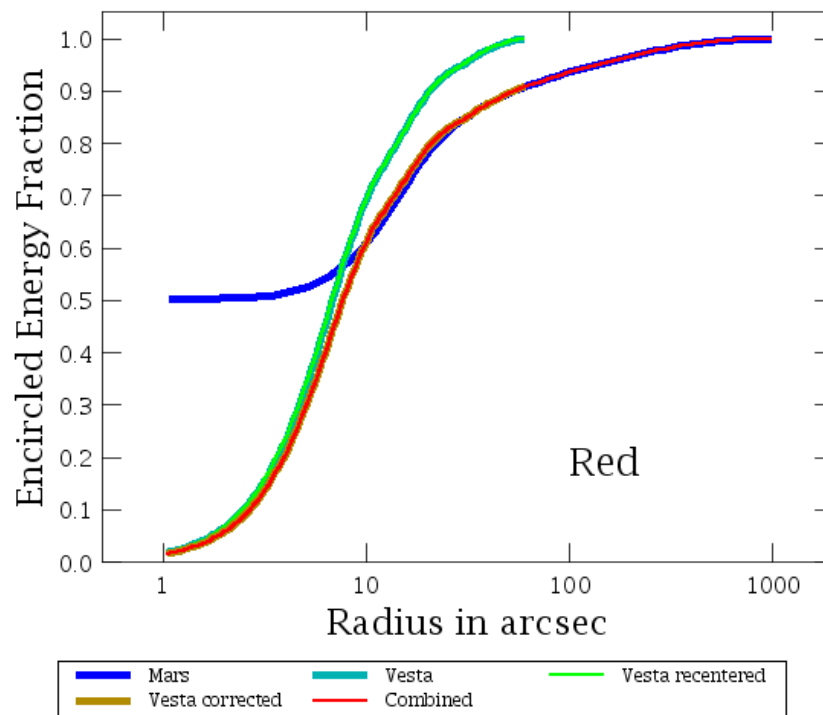


Figure 28: Encircled Energy Fraction for red. Contributing Mars and Vesta data are shown along with the final combination.

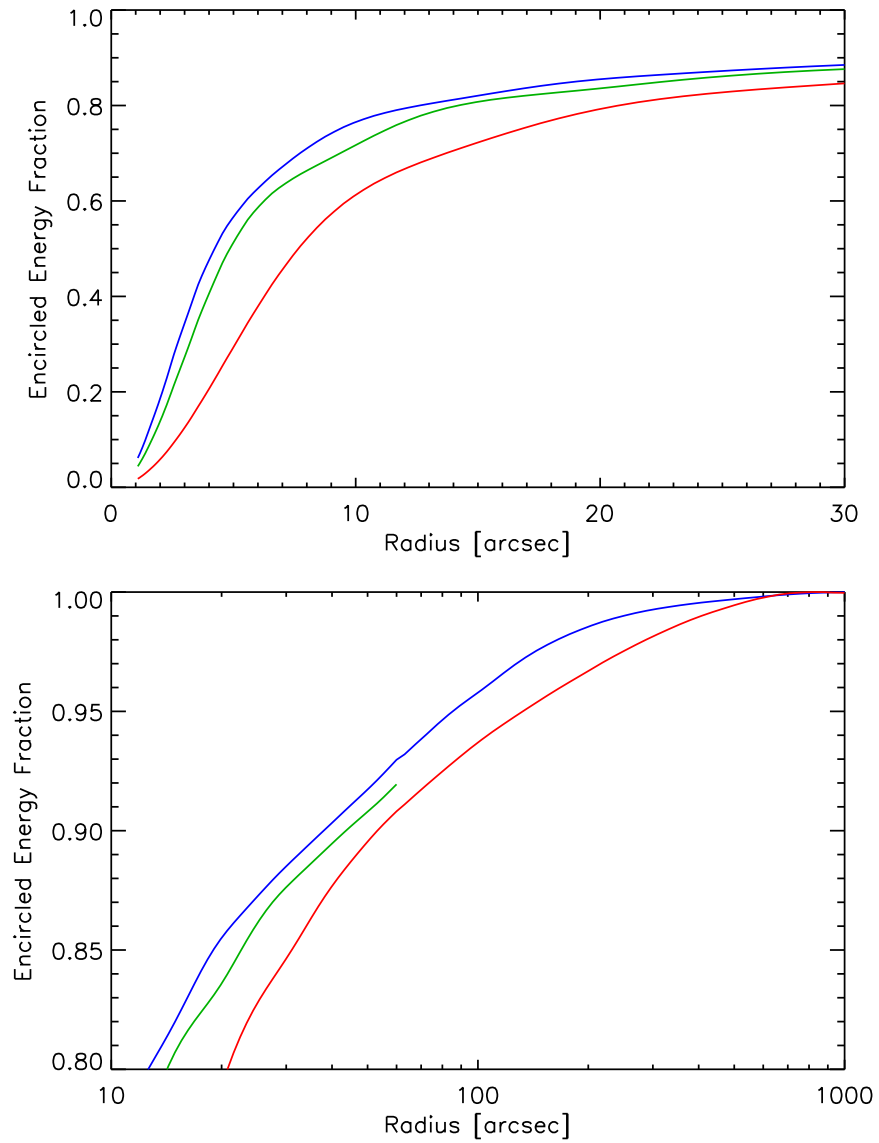


Figure 29: Combined Encircled Energy Fractions for all three PACS bands

9 Data products accompanying this note

Tarball PACSPSF_PICC-ME-TN-033_v1.0.tar.gz contains the following data:

- Vesta PSFs from OD160 and OD345 data. All are processed with a masking radius 60 arcsec and explicitly subtracting the background at $r=61-70$ arcsec. Total signal inside $r=60$ is normalized. File names follow a scheme Band_speed_source_OD_OA_remarks.fits e.g. red_20_vesta_od160_OA+63_recentered.fits, where OD is the operational day the data were taken and OA the scan orientation angle in degrees in the array frame, as entered into HSPOT. For blue and green there is a 1:1 correspondence to OBSIDs in the observation summary table above, while the red data average data from equivalent blue+red and green+red OBSIDs. Note that the Vesta observations from these ODs are publicly available from the Herschel Science Archive for experiments on the effect of other reduction schemes or parameters.
- Blue, green and red EEF curves from the combination of Vesta and Mars data. Columns in the files combinedEEF_blue.txt etc. are (1) Radius in arcsec (2) Encircled fraction of the energy out to $r=1000$ arcsec (3) Uncorrected Vesta EEF out to $r=60$ arcsec. Note that the current PACS flux calibration (Responsivity calfile FM 5) was derived using EEFs based on version 0.3 of this note, which are missing large radius flux. These EEFs are conceptually equivalent to column 3 of the current release.

The individual files in PACSPSF_PICC-ME-TN-033_v1.0.tar.gz are:

```
blu_10_vesta_od160_OA+63.fits
blu_10_vesta_od160_OA+63_recentered.fits
blu_20_vesta_od160_OA+63.fits
blu_20_vesta_od160_OA+63_recentered.fits
blu_20_vesta_od345_OA+42.fits
blu_20_vesta_od345_OA+42_recentered.fits
blu_20_vesta_od345_OA-42.fits
blu_20_vesta_od345_OA-42_recentered.fits
blu_20para_vesta_od160_OA+63_recentered.fits
blu_20para_vesta_od345_OA+42_recentered.fits
blu_20para_vesta_od345_OA-42_recentered.fits
blu_60_vesta_od160_OA+63.fits
blu_60_vesta_od160_OA+63_recentered.fits
blu_60_vesta_od345_OA+42.fits
blu_60_vesta_od345_OA+42_recentered.fits
blu_60_vesta_od345_OA-42.fits
blu_60_vesta_od345_OA-42_recentered.fits
blu_60para_vesta_od160_OA+63_recentered.fits
blu_60para_vesta_od345_OA+42_recentered.fits
blu_60para_vesta_od345_OA-42_recentered.fits
combinedEEF_blue.txt
combinedEEF_green.txt
combinedEEF_red.txt
grn_10_vesta_od160_OA+63.fits
grn_10_vesta_od160_OA+63_recentered.fits
grn_20_vesta_od160_OA+63.fits
grn_20_vesta_od160_OA+63_recentered.fits
grn_20_vesta_od345_OA+42.fits
```


grn_20_vesta_od345_0A+42_recentered.fits
grn_20_vesta_od345_0A-42.fits
grn_20_vesta_od345_0A-42_recentered.fits
grn_20para_vesta_od160_0A+63_recentered.fits
grn_20para_vesta_od345_0A+42_recentered.fits
grn_20para_vesta_od345_0A-42_recentered.fits
grn_60_vesta_od160_0A+63.fits
grn_60_vesta_od160_0A+63_recentered.fits
grn_60_vesta_od345_0A+42.fits
grn_60_vesta_od345_0A+42_recentered.fits
grn_60_vesta_od345_0A-42.fits
grn_60_vesta_od345_0A-42_recentered.fits
grn_60para_vesta_od160_0A+63_recentered.fits
grn_60para_vesta_od345_0A+42_recentered.fits
grn_60para_vesta_od345_0A-42_recentered.fits
red_10_vesta_od160_0A+63.fits
red_10_vesta_od160_0A+63_recentered.fits
red_20_vesta_od160_0A+63.fits
red_20_vesta_od160_0A+63_recentered.fits
red_20_vesta_od345_0A+42.fits
red_20_vesta_od345_0A+42_recentered.fits
red_20_vesta_od345_0A-42.fits
red_20_vesta_od345_0A-42_recentered.fits
red_60_vesta_od160_0A+63.fits
red_60_vesta_od160_0A+63_recentered.fits
red_60_vesta_od345_0A+42.fits
red_60_vesta_od345_0A+42recentered.fits
red_60_vesta_od345_0A-42.fits
red_60_vesta_od345_0A-42recentered.fits

10 Related documents

Review on PACS bolometers time constant, Billot et al., SAP-FIRST-NB-0688-05 (expectations for PSF smearing by fast scan)

PACS Test Analysis Report FM-ILT - Part III PICC-ME-TR-007 Section 3.1.4 (D.Lutz) on Photometer Point Spread Function

Herschel/PACS modelled point-spread functions, N. Geis and D. Lutz, PICC-ME-TN-029 issue 2.0

In-orbit crosstalk in the PACS photometer, PICC-ME-TN-034

Herschel straylight report, in preparation by the Herschel Straylight Working Group

PACS spatial coordinates cheat-sheet, PICC-ME-TN-027

11 Document change record

Version	Date	Initials	Comment
0.1	2009-09-16	DL	Quick version
0.2	2009-10-27	DL	Added OD160 Vesta
0.3	2009-11-10	DL	Minor updates to Vesta psf, bright source morphology
1.0	2010-10-22	DL	Major rewrite, based on 5.0 re-reduction
1.01	2010-11-03	DL	Added list with tarball contents